AD-A214 866

REPORT DOCUMENTATION PAGE

Form Approved
OMB No. 0704-0188

1. AGENCY USE ONLY (Leave blank)	2. REPORT DATE	3. REPORT TYPE AND DATES COVERED
	January 1982	Final (1 Jan 81-31 Dec 81)

4. TITLE AND SUBTITLE
MECHANICAL RESPONSE OF MATERIALS WITH PHYSICAL DEFECTS
PART 2: COMBINED MODELING OF MATERIAL DAMAGE AND CRACK PROPAGATION FOR CENTER CRACKED PANEL

5. FUNDING NUMBERS
61102F
2307/B1

6. AUTHOR(S)
G.C. Sih
P. Matic

7. PERFORMING ORGANIZATION NAME(S) AND ADDRESS(ES)
Institute of Fracture and Solid Mechanics
Lehigh University
Bethlehem, PA 18015

8. PERFORMING ORGANIZATION REPORT NUMBER
AFOSR-TR- 89-1466

9. SPONSORING/MONITORING AGENCY NAME(S) AND ADDRESS(ES)
AFOSR
BLDG 410
BAFB DC 20332-6448

10. SPONSORING/MONITORING AGENCY REPORT NUMBER
F49620-81-K-0005

11. SUPPLEMENTARY NOTES

12a. DISTRIBUTION/AVAILABILITY STATEMENT
Approved for public release;
distribution unlimited.

12b. DISTRIBUTION CODE

13. ABSTRACT (Maximum 200 words)

14. SUBJECT TERMS	15. NUMBER OF PAGES	16. PRICE CODE
	51	

17. SECURITY CLASSIFICATION OF REPORT	18. SECURITY CLASSIFICATION OF THIS PAGE	19. SECURITY CLASSIFICATION OF ABSTRACT	20. LIMITATION OF ABSTRACT
unclassified	unclassified		

DISCLAIMER NOTICE

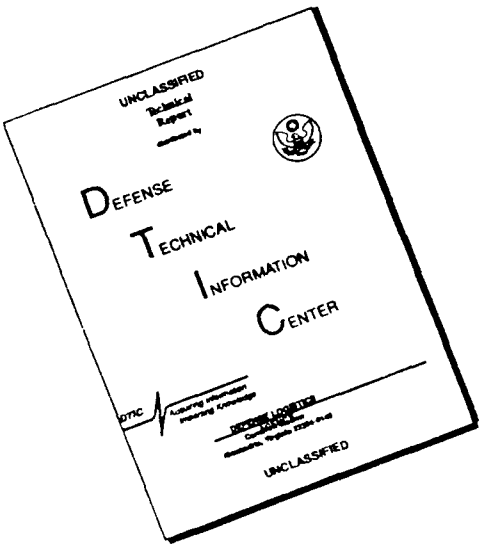

THIS DOCUMENT IS BEST QUALITY AVAILABLE. THE COPY FURNISHED TO DTIC CONTAINED A SIGNIFICANT NUMBER OF PAGES WHICH DO NOT REPRODUCE LEGIBLY.

F49620-81-K-0005

MECHANICAL RESPONSE OF MATERIALS WITH PHYSICAL DEFECTS
PART 2: COMBINED MODELING OF MATERIAL DAMAGE AND CRACK PROPAGATION FOR CENTER CRACKED PANEL

BY

G. C. SIH AND P. MATIC

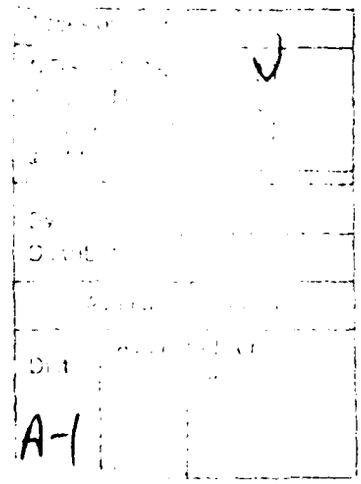

FINAL TECHNICAL REPORT
AFOSR-TR-82-2

JANUARY 1982

AIR FORCE OFFICE OF SCIENTIFIC RESEARCH
BOLLING AIR FORCE BASE, D.C. 20332

MECHANICAL RESPONSE OF MATERIALS WITH PHYSICAL DEFECTS

PART 2: COMBINED MODELING OF MATERIAL DAMAGE AND CRACK PROPAGATION FOR CENTER CRACKED PANEL

by

G. C. Sih and P. Matic

Institute of Fracture and Solid Mechanics

Lehigh University

February 1982

ABSTRACT

This is the second part of an investigation dealing with the global load-displacement behavior of a center cracked panel. Energy dissipating mechanisms of microcrack formation and macrocrack propagation are modeled separately and in combination in accordance with a predetermined criterion providing the limits for each mechanism. Nonlinear global behavior of the cracked panel is exhibited on the load-displacement curve developed by incremental loading and macrocrack growth with or without microcrack damage.

The regions of microcrack initiation to the sides of the macrocrack are assumed to coincide with the locations of maximum strain energy density $(\Delta W/\Delta V)_{max}$ condition similar to that of Haigh and Beltrami for yielding. The material elements within these regions modeled by the finite element grids undergo a decrease in the local stiffness which reflects the severity of damage. The damage threshold for each element corresponds to the elastic strain energy density at the yield stress level of a uniaxial tensile test specimen. As the material elements are damaged, the initial linearly elastic behavior changes to pseudo-linear elastic behavior, under the assumption that any energy dissipated due to microcrack generation is no longer recoverable upon unloading. No other dissipative mechanism of microdamage is assumed. The proposed Multiple Damage model describes the local effect of microcracking by a finite element formulation that utilizes twenty-four (24) discrete values of the secant elastic modulus of a specified uniaxial tensile true stress-true strain curve. The most severe level of material damage corresponds to a secant modulus evaluated from the point of ultimate stress and strain. This represents the effective properties of the microcracked portion of the medium.

The direction of macrocrack growth is also assumed to be governed by the Strain Energy Density Theory. In contrast to microdamage, the locations of $(\Delta W/\Delta V)_{min}$ determines macrocrack advance. The increment of crack growth at a given load depends on the critical magnitude of $\Delta W/\Delta V$ characteristic of the material ahead of the crack front and is designated by $(\Delta W/\Delta V)_c$ in the absence of damage at the microscopic level. Otherwise, the local stiffness of the material along the path of expected crack growth may also be affected and should be distinguished accordingly with a different notation $(\Delta W/\Delta V)_c^*$. The value of $(\Delta W/\Delta V)_c^*$ is a relative value which represents the decreased resistance to fracture indicative of the degree of material damage. This is consistent with those situations where microdamage ahead of the macrocrack precedes the macrocrack propagation. The material is weakened in that less energy is required to advance the crack front which corresponds to a reduction in $(\Delta W/\Delta V)_c$.

The applied load is considered as the independent variable which increased incrementally while material damage at both the microscopic and macroscopic level is monitored by the model described above. The stress and failure analysis is repeated for each increment of macrocrack growth. This could be done up to the point of fracture termination that is the final total separation of the panel, assuming that the material parameter governing crack instability is known. The results for two different fracture toughnesses are displayed graphically and discussed in terms of the degree of load-displacement nonlinearity caused by nonuniform crack growth rate and change of local stiffness of the material owing to microcracking. It is found that the individual contribution of these two effects depends on the fracture toughness of the material while the loading rate was kept constant.

INTRODUCTION

The interaction of material damage at the microscopic level accompanied by macrocracking in engineering materials is of fundamental interest. A basic understanding of this can lead to an extension of the admissible range of allowable load for structural components. This requires the identification of the successive failure modes with the load history of a given structural component which behaves in a ductile manner. The optimization of strength and ductility cannot be achieved without a consistent and reliable procedure that can qualitatively and quantitatively account for the path dependent material damage process. This involves a description of slow and fast crack growth. It is well-known that the local stiffness of a material is reduced when yielding takes place. Microphotography of the yielded materials [1] shows that mechanical imperfections in the form of minute cracks or cavities are formed which, in this investigation, will be referred to as microdamage. This type of damage that has been commonly observed in regions close to the macrocrack front can significantly influence the growth characteristics of the macrocrack and the load at fracture instability.

The classical continuum theory of plasticity has not had much success to explain the foregoing physical damage process for a number of reasons. One of them is that the yield condition, say the Huber or Henky-von Mises criterion, is chosen independent of the fracture initiation and/or propagation condition of the macrocrack [2,3]. This can introduce a large degree of inconsistency and arbitrariness into the stress and failure analysis. An attempt is made here to model microscopic material damage near a macrocrack by a finite element procedure in which the local stiffness at the different locations change in accordance with the strain energy density criterion that can uniquely predict microdamage or yielding as well as the growth of the macrocrack. It has been established pre-

viously [4,5] that the relative maximums of $\Delta W/\Delta V$ correspond to yielding and the relative minimums to fracture. In this way, a consistent procedure can be developed to model material damage by a combination of fracture and yielding, a situation often desired in engineering structural application.

PHYSICAL MODEL: A CRACKED SPECIMEN

In order to exhibit the amount of irreversibility caused by physical damage of the loaded material, the behavior of a center cracked panel, Figure 1, under unidirectional tensile loading perpendicular to the crack is depicted. Such a specimen features a macro-defect in the form of a symmetrically located crack, whose length is of the same order of magnitude as the specimen size. Under sufficiently high loads, the macrocrack would be expected to increase in length. For some value of the load, the process will become unstable and result in failure of the panel.

A specimen made of a "ductile" material would be expected to develop damage at a lower scale level in the form of microcracks and/or microvoids. These defects may be initially present in the material, or may coalesce from the movement of dislocations and other defects at an even smaller scale, i.e., the atomic scale. In the presence of a macrocrack, such regions are known to exist ahead of the crack tip on both sides of a two-ended crack. The latter regions, commonly identified as "plastic enclaves" in the classical theory of plasticity, have been the subject of much attention since the dimensions of such regions can be significant when compared to the crack length. The microcracks themselves will produce microplastic regions ahead of both crack tips, also. Their effect on the propagation of the macrocrack is not yet fully understood.

In order to develop a model of the processes described above, it is assumed that the strain energy density, dW/dV, per unit volume of material, is the quantity that reflects material damage at the micro level, as well as the length and direction of macrocrack propagation at the macro level. The term "material damage" will refer to processes which utilize strain energy at the continuum scale

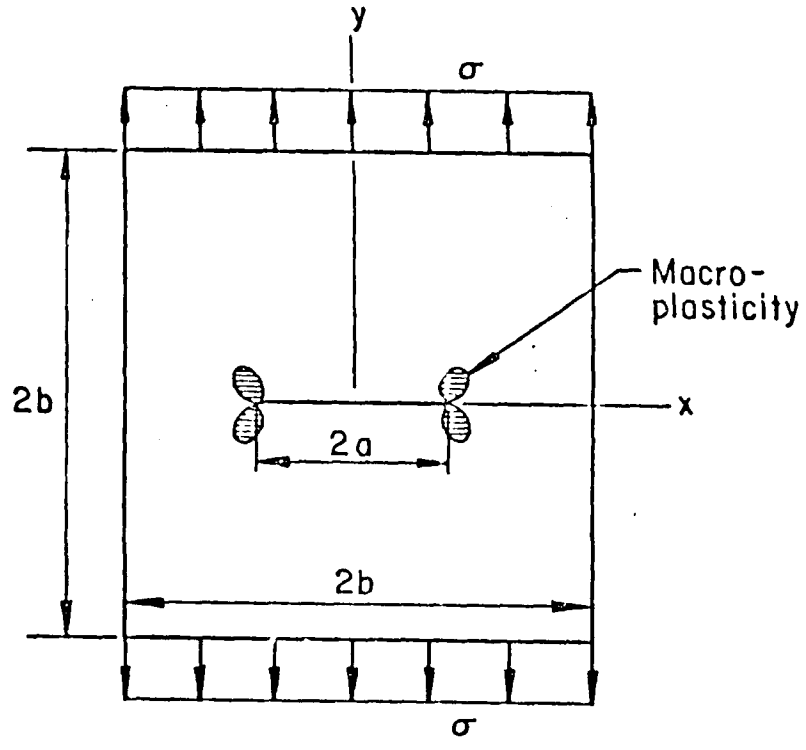

Applied Load $p = 2\sigma tb$ $a = 1.5"$

Thickness $t = 1.0"$ $b = 4.0"$

$a/b = 0.375$

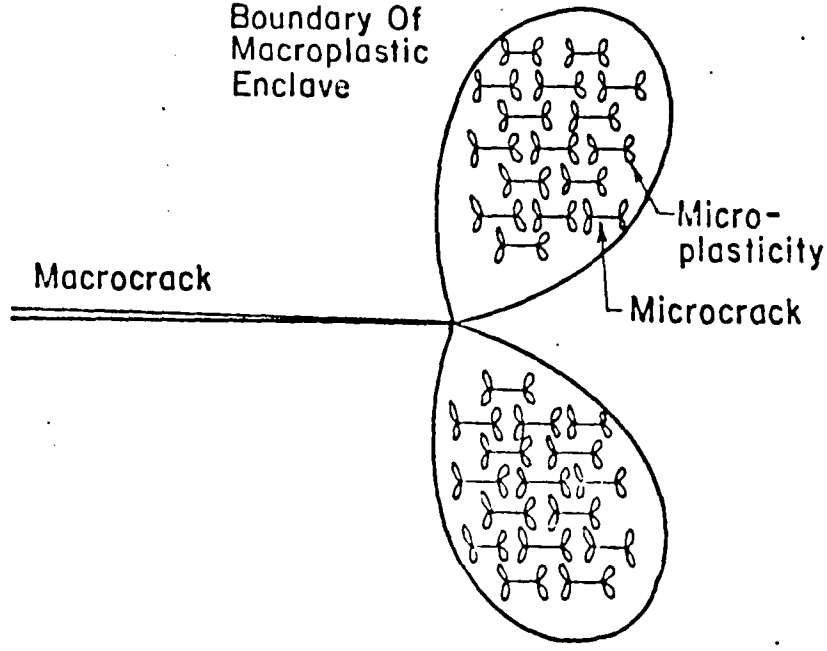

Schematic Detail Of Crack Tip In Ductile Material

Figure 1 - Center cracked panel specimen

to produce irreversible changes in the material. These changes will, in turn, affect the local material behavior as a result of the formation of microcracks, microvoids or coalescence of these defects. A survey of the effective material properties of bodies with statistically isotropic microcrack arrays is discussed in the first part of this report [6].

What is essential is to establish a unique correspondence between each point on a load displacement curve while the cracked panel is damaged by the build up of microcracks in the zones referred to as "macro-plasticity" in Figure 1 and the advancement of the macrocrack. The results will be informative for developing constitutive relations of different crystalline materials characterized by the different degrees of microdamage and macrocracking. In particular, it may be possible to distinguish those constitutive coefficients associated with describing material behavior from those characterizing material properties. For instance, the Young's modulus and Poisson's ratio are the only two material constants for an isotropic elastic-plastic material while the nonlinear behavior is described by the strain hardening exponents which are sensitive to change in specimen sizes.

FINITE ELEMENT FORMULATION

All stress analysis used to generate the load-displacement curves were carried out on center cracked panel specimens for materials with characteristics of a low yield stress (σ_y = 35,000 psi) structural steel. The load-displacement curves were calculated incrementally in a series of "stress analysis-material microdamage assessment-stress analysis-macrocrack extension" increments or cycles.

The Axisymmetric/Planar Elastic Structures (APES) two-dimensional fracture mechanics and stress analysis finite element program [7] performed the stress analyses portion of each increment. The formulation of APES utilizes quad-12 elements which allow for cubic displacement fields and quadratic stress and strain fields within each element. The $r^{1/2}$ displacement field in the immediate vicinity of the crack tip is embedded in the solution through the use of 1/9 to 4/9 nodal spacing on the element sides adjacent to the crack tip. The tensile loading of the panel subjects the crack to a symmetric Mode I situation, thus requiring only one quarter of the physical problem, Figure 2, to be modeled by 440 nodes which define 77 elements. The CDC 6400 computer used in this study typically required 225 system seconds and 132k of central memory to complete the stress analysis for a given specimen load and damage distribution.

The microdamage processes that occur in the material manifest themselves by changes in the material properties at the continuum level. The finite element formulation allows for this by associating with each element one of up to 25 different material property pairs (i.e., elastic modulus E, and Poisson's ratio ν). Thus, a set of properties (E_1, ν_1) corresponding to the initial elastic behavior of the material, as defined from an uniaxial tensile test specimen, and up to 24 discrete material property pairs (E_i, ν_i) for i = 2,3,4,...,24, different instances

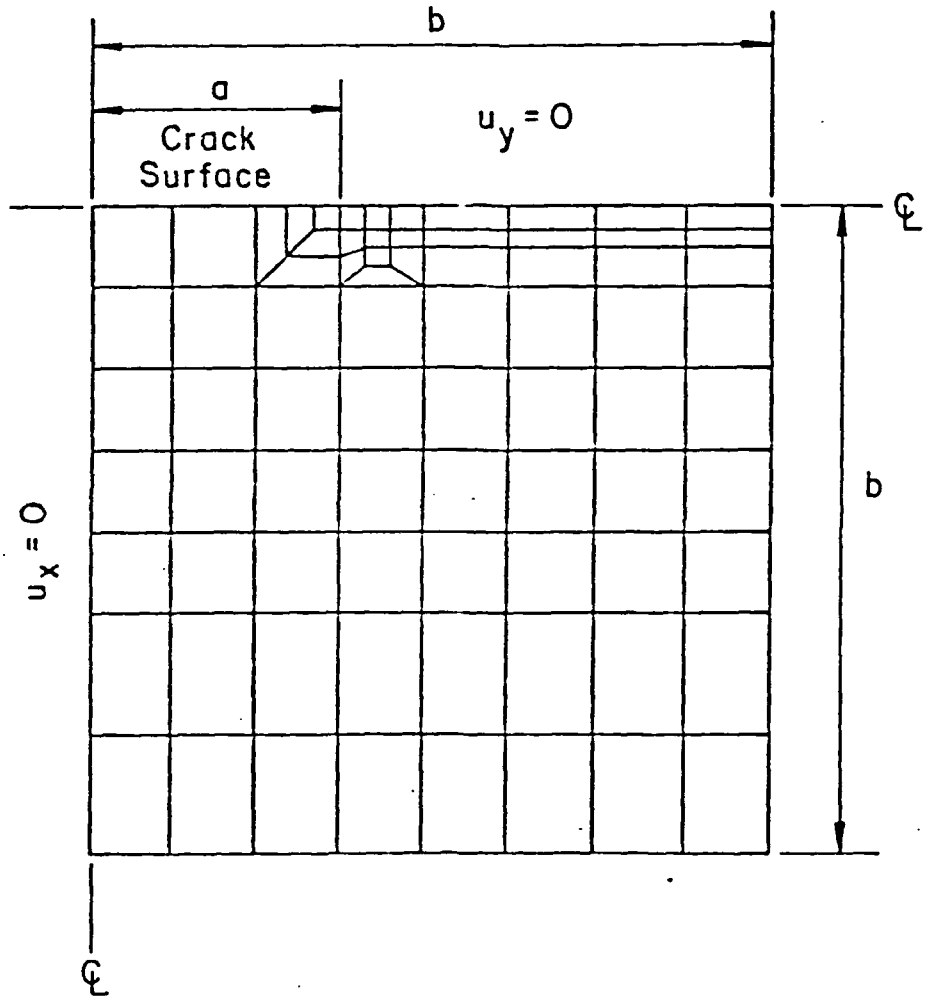

Figure 2 - Finite element grid

in the damaged material's developing history.

The extension of the macrocrack in Figure 1 is analyzed by convecting the grid boundaries in the finite element analysis for each increment of macrocrack growth. This is done so that the crack tip and surrounding region are not distorted when the crack grows. Otherwise, distortion of the finite elements would interfere with the grid pattern caused by material damage. Convection of the boundaries confines any element distortion to the boundary elements which are less likely to sustain microdamage at the loads considered.

MICRODAMAGE MODEL

The damage model used for the center cracked panel specimen was based on 24 discrete damage levels of the virgin material. (Recall that 25 different materials can be incorporated into the finite element formulation). This model will be referred to as the Multiple Damage Level Model. The 24 damage levels were defined on the basis of equal multiple elastic secant modulus reductions, Figure 3. The 24th is defined from the ultimate stress and strain, σ_u and ε_u, of the true stress-true strain curve. Since each of the 24 damage levels is attained at a different value of strain energy density, the true stress-true strain curve must be explicitly given, Figure 4. For this analysis, the form used was

$$\begin{aligned} \sigma &= E_1 \varepsilon \qquad \sigma < \sigma_y \\ \sigma &= A\varepsilon^n \qquad \sigma \geq \sigma_y \end{aligned} \tag{1}$$

For both materials, the stress-strain relations are

$$\begin{aligned} \sigma &= 30.0 \times 10^6 \, \varepsilon \qquad \sigma < \sigma_y \\ \sigma &= 190500 \, \varepsilon^{0.251} \qquad \sigma \geq \sigma_y \end{aligned} \tag{2}$$

which is based on a structural steel. For the onset of damage in the material, the strain energy density in the ith element must be greater than the strain energy density at the yield stress

$$\left(\frac{\Delta W}{\Delta V}\right)_i > \left(\frac{\Delta W}{\Delta V}\right)_y \tag{3}$$

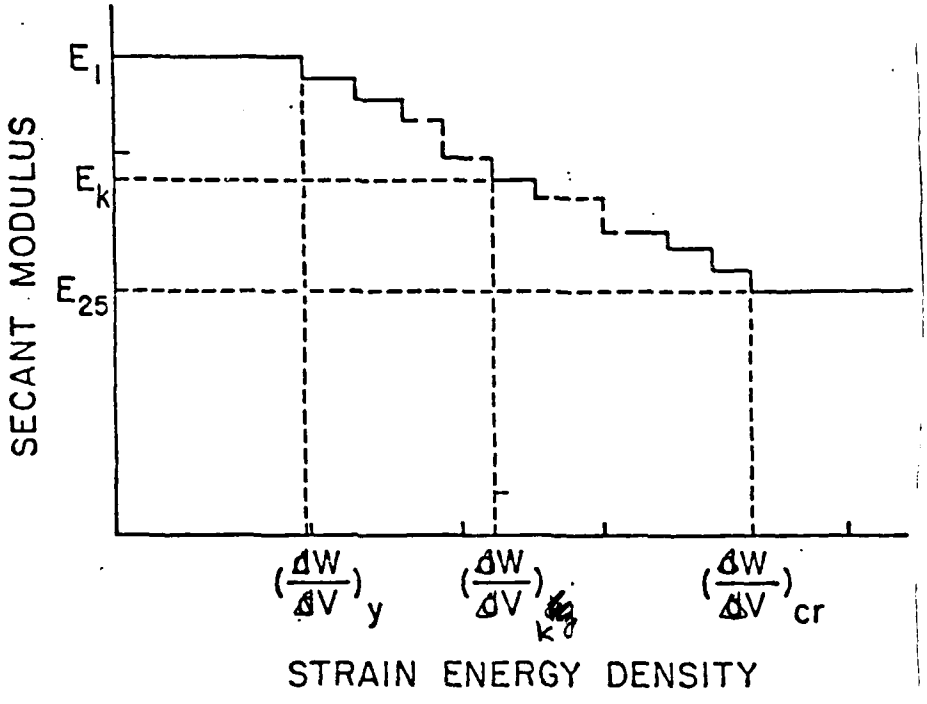

Figure 3 - Secant Modulus Versus Strain Energy Density

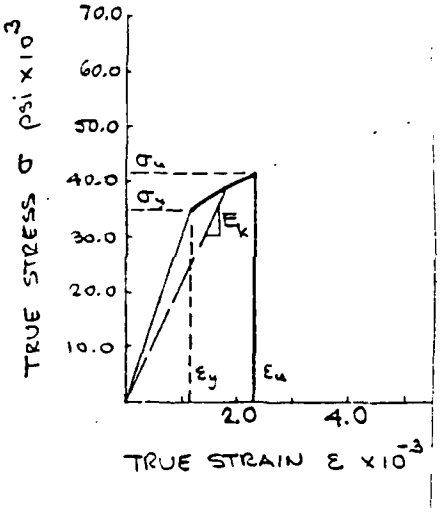

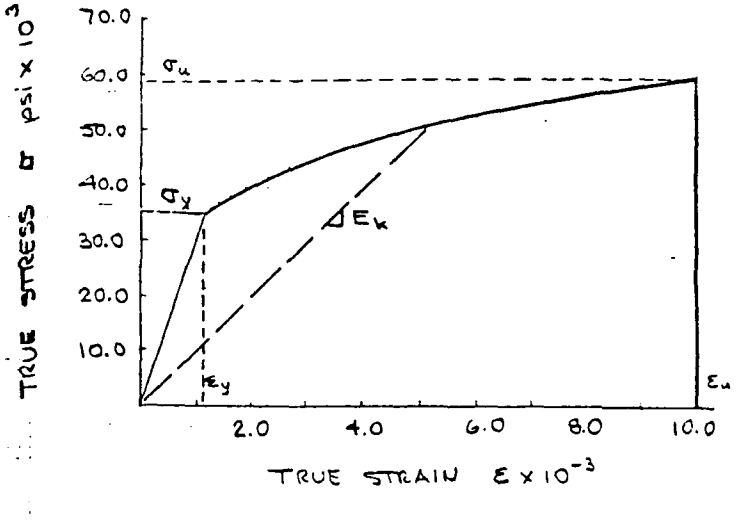

$\sigma = E_1 \varepsilon$ $\quad \sigma < \sigma_y$

$\sigma = 190500\, \varepsilon^{0.251}$ $\quad \sigma \geq \sigma_y$

$E_1 = 30.0 \times 10^6$ psi
$E_{25} = 18.0 \times 10^6$ psi
$\sigma_y = 35{,}000$ psi
$\sigma_u = 41{,}500$ psi
$(\Delta W/\Delta V)_y = 20.4$ lb-in/in³
$(\Delta W/\Delta V)_{cr} = 64.2$ lb-in/in³

$E_1 = 30.0 \times 10^6$ psi
$E_{25} = 6.0 \times 10^6$ psi
$\sigma_y = 35{,}000$ psi
$\sigma_u = 59{,}900$ psi
$(\Delta W/\Delta V)_y = 20.4$ lb-in/in³
$(\Delta W/\Delta V)_{cr} = 466.7$ lb-in/in³

Figure 4 Uniaxial True Stress - True Strain Curves

where the strain energy density for the case of plane strain is given by

$$\frac{\Delta W}{\Delta V} = \frac{\sigma_x^2}{2E} + \frac{\sigma_y^2}{2E} - \frac{\nu\sigma_x\sigma_y}{E} + \frac{\tau_{xy}^2}{2G} \tag{4}$$

For the k$_{th}$ level of damage in the material, characterized by an elastic modulus of E_k, the strain energy density in the ith element must be

$$\left(\frac{\Delta W}{\Delta V}\right)_k < \left(\frac{\Delta W}{\Delta V}\right)_i \leq \left(\frac{\Delta W}{\Delta V}\right)_{k+1} \tag{5}$$

where, for the form of the given stress-strain relation

$$\begin{aligned}\left(\frac{\Delta W}{\Delta V}\right)_k &= \int_0^{\varepsilon_k} \sigma d\varepsilon = \int_0^{\varepsilon_y} \sigma d\varepsilon + \int_{\varepsilon_y}^{\varepsilon_k} \sigma d\varepsilon \\ &= \left(\frac{\Delta W}{\Delta V}\right)_y + \frac{A}{n+1}\left(\varepsilon_k^{n+1} - \varepsilon_y^{n-1}\right) \\ &= \frac{1}{2}\frac{\sigma_y^2}{E_1} + \frac{A}{n+1}\left(\varepsilon_k^{n+1} - \varepsilon_y^{n-1}\right)\end{aligned} \tag{6}$$

The load P is the independent variable for this model, since all elements have the potential to sustain damage at a given load. The increment of the load P can be arbitrarily chosen within the limits of upper and lower bounds as described in [6].

The concept of the mean damage level $\bar{d}$ and damage center $(\bar{x}_d, \bar{y}_d)$ have been introduced in order to quantify the damage zone in terms of a scalar magnitude and its position in the panel specimen. The mean damage level $\bar{d}$ is defined on the basis of the discrete reductions in elastic modulus. Defining the damage in the ith element as the fractional reduction in the elastic modulus by

$$d_1 = \frac{E_1 - E_k}{E_1} \tag{7}$$

The mean damage level $\bar{d}$ is calculated as

$$\bar{d} = \frac{1}{V_i} \sum_i d_i V_i \tag{8}$$

Elements which have not reached the $(dW/dV)_y$ damage threshold, of course, have values of d_i equal to zero. The coordinates $(\bar{x}_d, \bar{y}_d)$ of the damage center are defined on the basis of the first moment of the damage distribution

$$\bar{x}_d = \frac{1}{\sum_i d_i V_i} \sum_i \bar{x}_i d_i V_i$$

$$\bar{y}_d = \frac{1}{\sum_i d_i V_i} \sum_i \bar{y}_i d_i V_i \qquad i = 1,2,\ldots,n_d \tag{9}$$

where n_d is the number of elements having damage at the applied load. This is simply the discretized form of first moment integrals with the density function taken to be the damage level. The $\bar{x}_i$ and $\bar{y}_i$ coordinates are the coordinates of the ith element centroid.

The locus of the damage center coordinates at each load serves as an indication of how the material damage, as defined by the models incorporated here, is being distributed in the center cracked panel. The crack tip is the origin of the locus of points, and the subsequent curve is indicative as to whether the lower levels of damage at the periphery of the damage zone, or the higher levels nearer to the crack tip are predominating the damage accumulation process at a given load increment. Also, the effect of the free boundary ahead of the crack can be evaluated as to its ability to influence the damage zone's direction of

propagation. Typically, one would expect the damage zone boundary to propagate more toward the free surface as the zone size becomes significant with respect to the uncracked ligament length.

STRAIN ENERGY DENSITY THEORY OF MACROCRACK PROPAGATION

Strain Energy Density Theory, as proposed by Sih [4,5], makes use of the energy state and material properties ahead of the crack for predicting the direction and increment of crack growth. Physically, the material behavior in the immediate vicinity of the crack tip is too complex to be described by a continuum mechanics analysis because of the influence of material microstructure. This necessitates the investigation to be centered on elements at a finite distance away from the crack tip such that the material properties can be described by parameters at the continuum or macroscopic scale level.

The strain energy density field in the neighborhood of the crack tip has the form

$$\frac{dW}{dV} = \frac{1}{r}\,[S(a,\theta;\text{material properties})] + \text{nonsingular terms} \tag{10}$$

where r is the radial distance from the crack tip, a is the half crack length, θ is the angular position coordinate, and the function S is the strain energy density factor which is the coefficient of the r^{-1} singular energy density field. In the case of linear, homogeneous and isotropic elasticity, the strain energy density factor can be expressed in terms of the stress intensity factors k_1, k_2 and k_3 as

$$S = a_{11}k_1^2 + a_{12}k_1k_2 + a_{22}k_2^2 + a_{33}k_3^2 \tag{11}$$

where the a_{ij} $(i,j = 1,2,3)$ are functions of the elastic shear modulus, Poisson's ratio, and θ. The k_j-factors take the form

$$k_j = c_j \sigma\sqrt{a} \tag{12}$$

where the c_j are constants that depend on the solid geometry and σ is the loading. In the case of yielding, no realistic analytical crack tip stress or strain expressions* are available. Because of the nonhomogeneous nature of the elastic-plastic material behavior near the crack tip, a single parameter representation such as a stress intensity factor does not exist. Numerical calculation is required for analyzing the state of affairs near the crack tip.

A quasi-linear approach is taken such that each segment of crack growth accompanied by microdamage is analyzed using the $1/\sqrt{r}$ singularity solution. The global response consisting of all the increments of crack growth is nonlinear because the material will not be damaged uniformly around the crack. This effect is assessed quantitatively by a numerical procedure calculating the local strain energy density field.

The fundamental hypotheses of the strain energy density theory applied to both fracture and yielding may be stated as follows:

(I) Yielding is assumed to coincide with the location of relative maximum of $\Delta W/\Delta V$, i.e., $(\Delta W/\Delta V)_{max}$ and to occur when $(\Delta W/\Delta V)_{max}$ reaches a critical value $(\Delta W/\Delta V)_y$.

*Available solutions [8] assume that the material yields uniformly around the crack tip, a situation that deviates far from reality.

(II) Fracture is assumed to be determined by the location of relative m .imum of $(\Delta W/\Delta V)$, i.e., $(\Delta W/\Delta V)_{min}$ and to occur when $(\Delta W/\Delta V)_{min}$ reaches a critical value* $(\Delta W/\Delta V)_c$.

*As mentioned earlier, if the material along the prospective fracture path is also yielded or damaged microscopically, then the critical value must be modified as $(\Delta W/\Delta V)_c^*$ depending on the severity of material damage.

STRESS AND FAILURE ANALYSIS

The development of damage zones and the propagation of a macrocrack are two irreversible damage processes which must be included to model the behavior of a real ductile material. Since material damage is a load history dependent process, stress and failure analysis must be performed in tandem for each increment of loading. Referring to the cracked panel in Figure 1, the load is increased until the strain energy density function $(\Delta W/\Delta V)$ for elements in the vicinity of the crack reaches a level corresponding to uniaxial tensile yield, i.e., $(\Delta W/\Delta V)_y$. Thus, a contour of $(\Delta W/\Delta V)_y$ = const. will be developed and enclose a larger region for each increment of loading. Macrocrack propagation is assumed to start when $(\Delta W/\Delta V)$ reaches a critical value $(\Delta W/\Delta V)_c$. As an example, if the macrocrack happens to advance into the undamaged material, the onset of macrocrack growth is

$$\left(\frac{\Delta W}{\Delta V}\right)_c^* = \left(\frac{\Delta W}{\Delta V}\right)_c \tag{13}$$

On the other hand, had damage already developed along the prospective fracture path, say by the amount $(\Delta W/\Delta V)_y$, then, the condition of macrocrack growth becomes

$$\left(\frac{\Delta W}{\Delta V}\right)_c^* = \left(\frac{\Delta W}{\Delta V}\right)_c - \left(\frac{\Delta W}{\Delta V}\right)_d \tag{14}$$

Equation (14) can thus be repeated for each successive increment of crack growth.

The relation of $(\Delta W/\Delta V)_d$ to $(\Delta W/\Delta V)_c^*$ for the tensile specimen is illustrated schematically in Figure 5. The area OYA represents the energy $(\Delta W/\Delta V)_d$ which

Figure 5 - Strain energy density definitions from uniaxial true stress-true strain curve

has been dissipated by the microdamage process due to loading along the stress strain curve up to point A. The relative critical strain energy density $(\Delta W/\Delta V)_c^*$ is the required amount of energy necessary for the critical strain energy density $(\Delta W/\Delta V)_c$ level to be reached in the material.

If the specimen were unloaded, the pseudo-linear elastic nature of the assumed material model would cause unloading to proceed along the line AO back to the origin. The area OAB is then the local recoverable elastic energy $(\Delta W/\Delta V)_e$. If loading were to continue further along curve AU, the additional energy required to reach $(\Delta W/\Delta V)_c$ is $(\Delta W/\Delta V)^*$ in view of equation (14). Thus, the relative critical strain energy density can also be expressed as the sum of the local recoverable and additional energy densities, i.e.,

$$(\Delta W/\Delta V)_c^* = (\Delta W/\Delta V)_e + (\Delta W/\Delta V)^* \tag{15}$$

To reiterate, microdamage is assumed to occur in the region local to the macrocrack front when a material element modeled by finite elements exceeds a certain limit $(\Delta W/\Delta V)_y$. Based on the strain energy density criterion, macrocrack growth begins when the relative minimum* of the strain energy density function reaches the condition in equation (14). The stable crack growth process continues until the condition of global instability

$$r_c^* \left(\frac{\Delta W}{\Delta V}\right)_c^* = S_c^* \tag{16}$$

is reached. The parameter r_c^* represents the last crack growth increment that corresponds to global instability and S_c^* may be interpreted as the fracture toughness of the material.

The load-displacement curves of the cracked panel are produced by successive applications of the APES finite element program for each load increment. This procedure incorporates the stress and failure analysis involving microdamage and crack propagation either separately or in combination with the method described above. A flow chart describing the step-by-step procedure is shown schematically in Figure 6.

*Even when the material surrounding the crack tip is completely yielded, the direction of crack initiation is still determined by $(\Delta W/\Delta V)_{min}$ calculated in the yielded material.

~~31~~

32

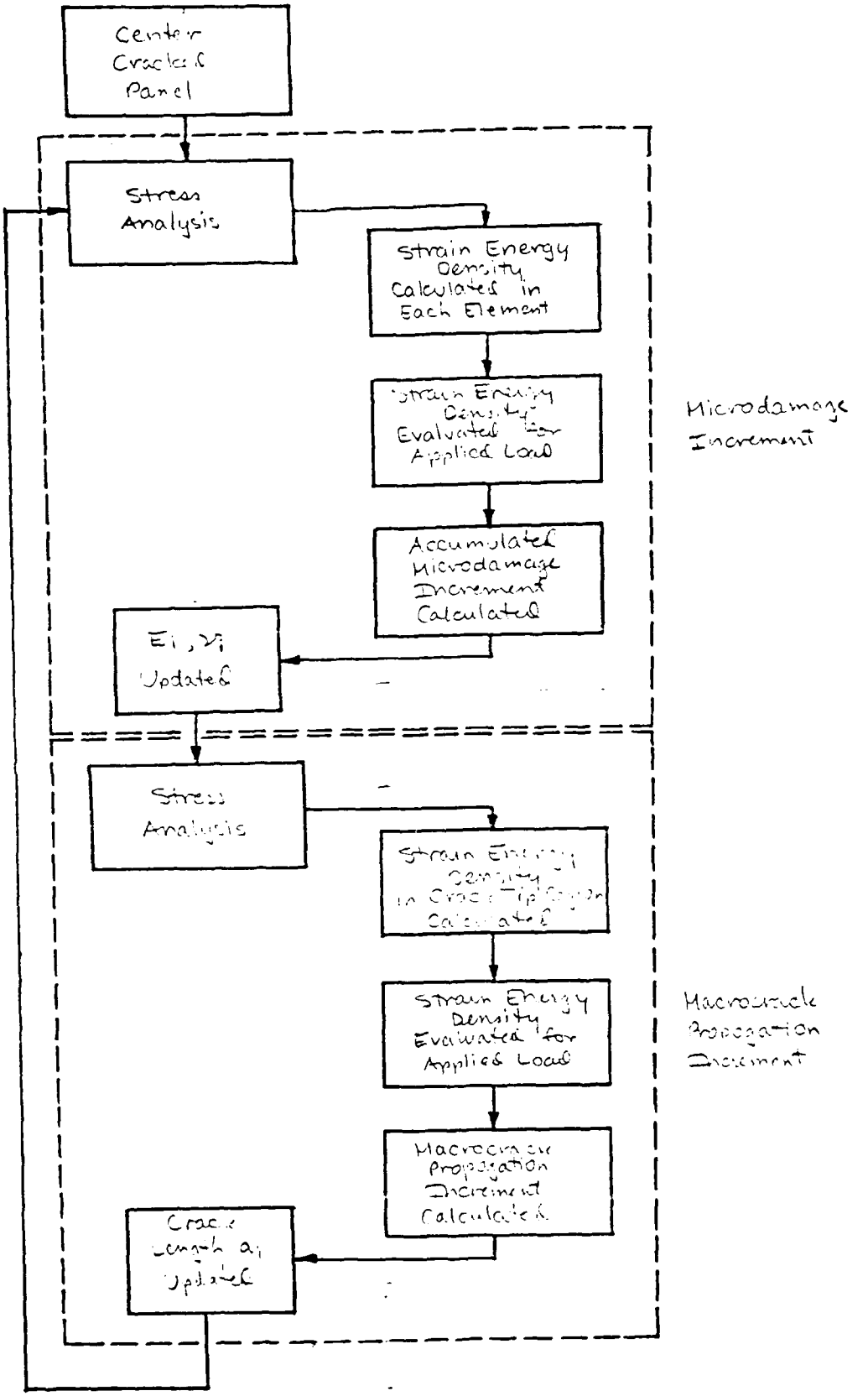

Figure 6 Combined Microdamage and Macrocrack Propagation Model

LOAD-DISPLACEMENT RESPONSE

The combined effects of microdamage and crack propagation on the incremental load-displacement curves are shown in Figure 7 for two materials with different $(\Delta W/\Delta V)_c$ values. The nonlinear response owing to damage is seen in terms of the departure of the curves from the linear response. According to the quasi-linear model, the difference of the nonlinear and linear responses of the panel with a material $(\Delta W/\Delta V)_c$ value of 466.7 lb-in/in^3 are seen to be approximately 60% of those for the panel with a material $(\Delta W/\Delta V)_c$ value of 64.2 lb-in/in^3.

In Figures 8 and 9, the separated and combined effects of microdamage and macrocrack propagation are shown for both materials. The nonlinear response of both panels due to the separate and combined effects of material damage at both scale levels are shown. As would be expected, the individual contributions of microdamage and macrocrack propagation are less than the combined effect. Of particular interest are the proportions of the individual effects for the two materials.

In the case of the less tough material, with $(\Delta W/\Delta V)_c$ = 64.2 lb-in/in^3, the global displacements are greater for macrocrack propagation alone with no microdamage as compared to the case of microdamage without crack propagation. Thus, microdamage appears to have less influence on the global panel stiffness than that due to crack propagation. For the high toughness material with $(\Delta W/\Delta V)_c$ = 466.7 lb-in/in^3, the reverse trend is observed. The microdamage effects, when taken alone, are seen to produce a greater reduction in global panel stiffness than macrocrack propagation.

The foregoing load-displacement curves were generated from $(\Delta W/\Delta V)_c$ values for the undamaged portion of the material as defined from the area under the uni-

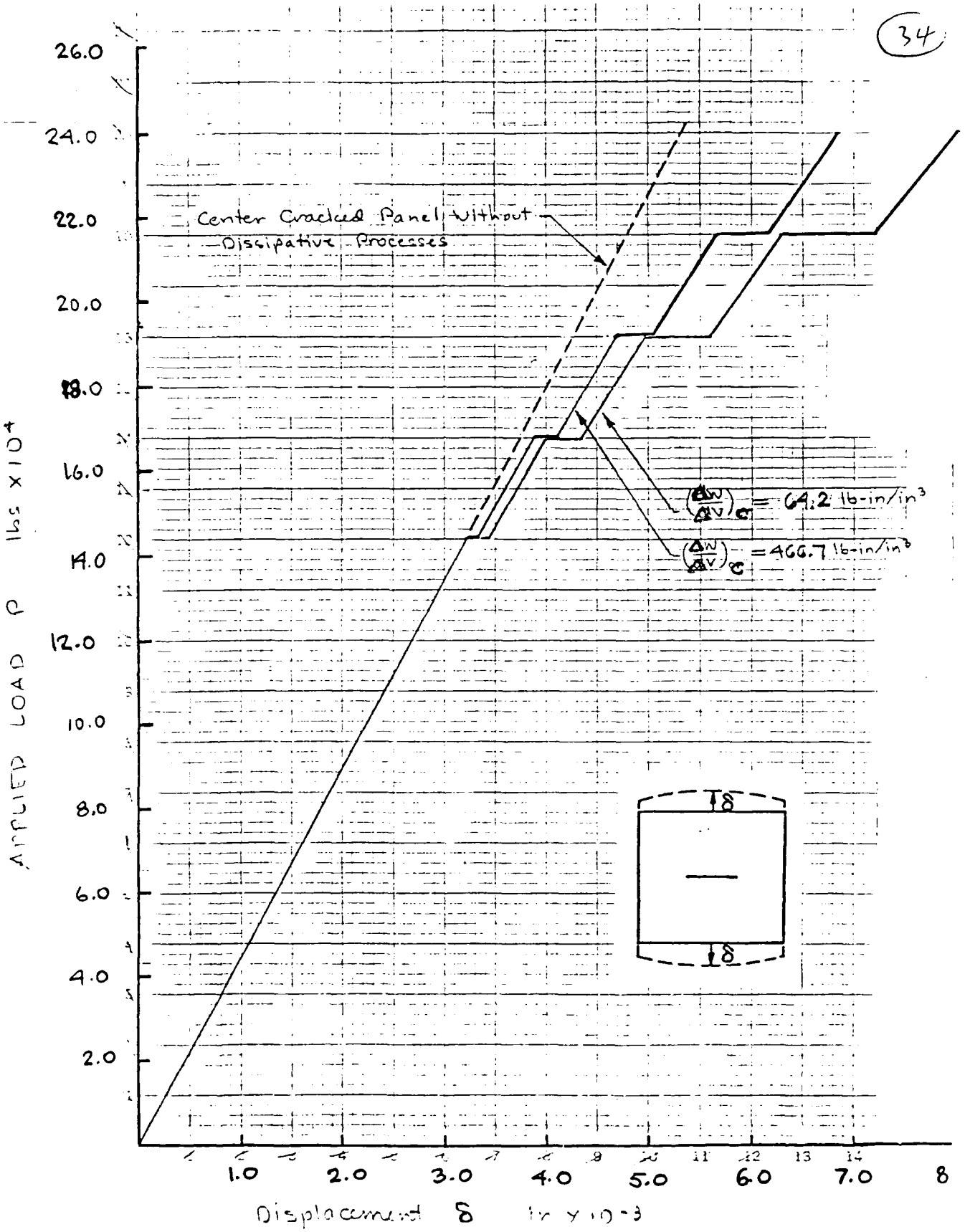

Figure 7 Load - Displacement [illegible]

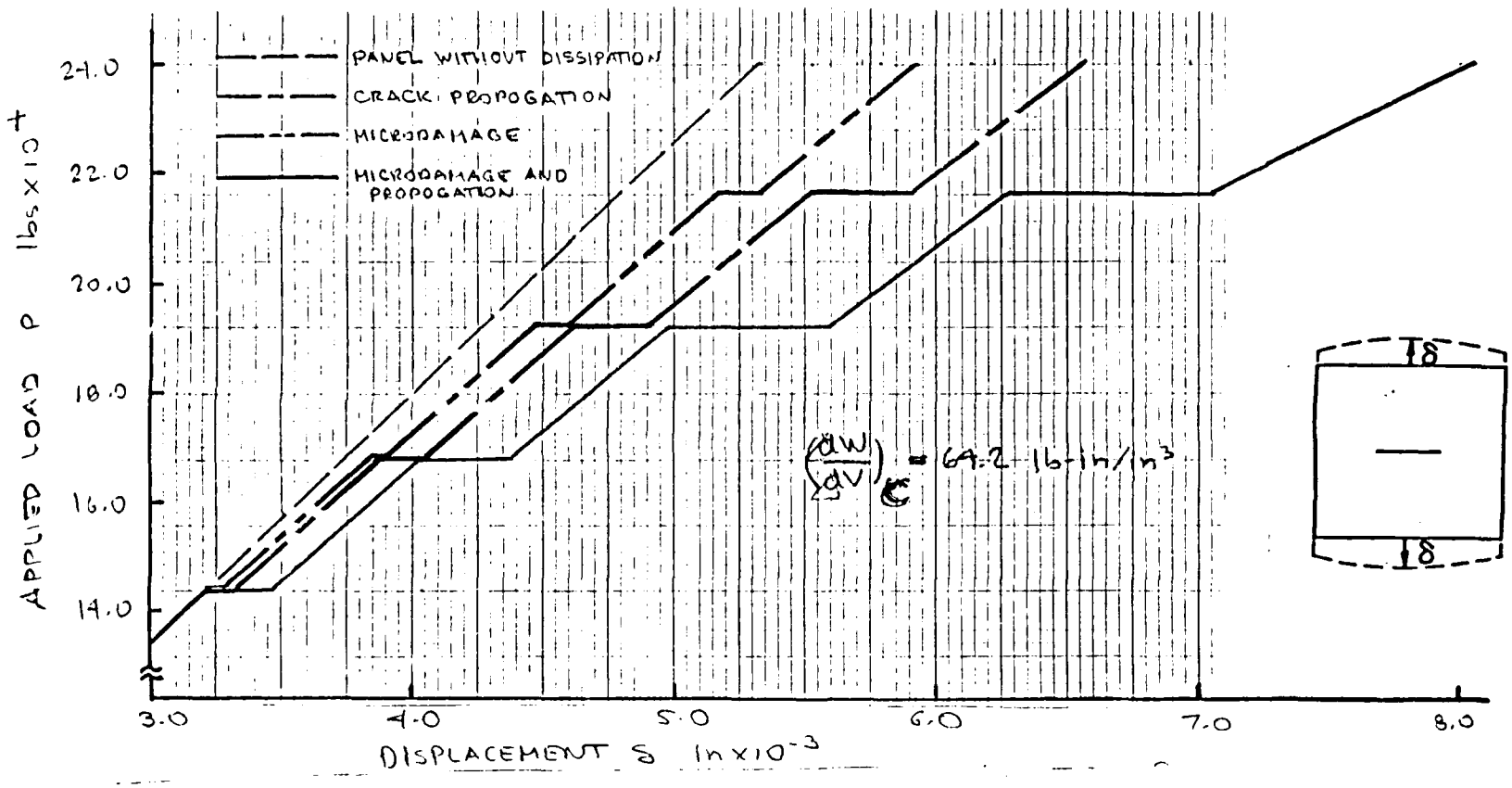

Figure 8 Seperate and Combined Effects of Microdamage and Macrocrack Propogation on Load-Displacement ... for $(dW/dV)_{cr}$ = 64.2 lb-in/in³

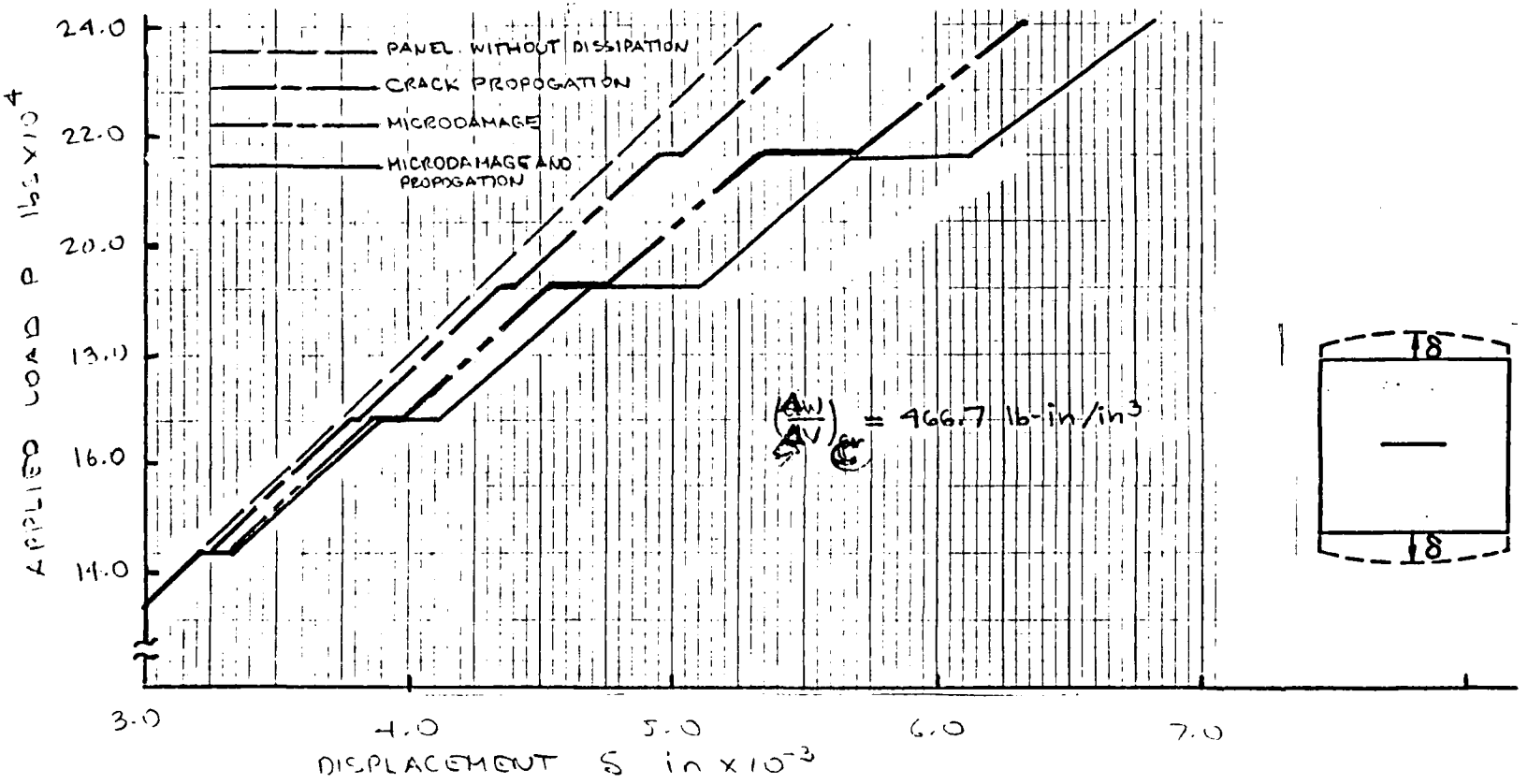

Figure 9 Combined and Seperate Effects of Microdamage and Macrocrack Propogation on Load-Displacement Curves for $(\Delta W/dV)_{cr}$ = 966.7 lb-in/in^3

axial true stress-true strain curves. While the microdamage process is a physically irreversible process, crack propagation is a sequence of material separation events contingent on the current damage distribution and relative critical strain energy density function $(\Delta W/\Delta V)_c^*$ throughout the material. Clearly, in a material with comparatively lower $(\Delta W/\Delta V)_c$, the damage process takes place over a narrower range of strain energy density values. In a material with higher $(\Delta W/\Delta V)_c$, this range of energies is greater, allowing for higher levels of damage prior to material degradation coincident with fracture.

The variations of global secant stiffnesses with load for microdamage and macrocrack propagation are shown in Figures 10 and 11. The comparative reduction in stiffness for the individual and combined effects of microdamage and crack propagation are again apparent. For a $(\Delta W/\Delta V)_c$ value of 64.2 lb-in/in^3, and at the maximum load considered, the effect of microdamage is seen to reduce the panel stiffness by ~10% while for the case of crack propagation, the stiffness is reduced by ~20%. The combined effects are greater than either taken individually, reducing the stiffness by ~33%. For a $(\Delta W/\Delta V)_c$ value of 466.7 lb-in/in^3, the stiffness reductions for microdamage, propagation and combined effects are approximately 16, 6 and 23%, respectively, at the maximum load considered. The relative influence of microdamage is seen to be greater than the effect of crack propagation, as discussed above on the basis of the load-displacement curves.

In Figures 12 and 13, the propagation of the macrocrack is shown in the absence of any microdamage. (For this reason, only a portion of the finite element grid is used to illustrate the propagation of the crack). This case corresponds to an ideally brittle material which fractures along flat surfaces. As would be expected, the crack propagates further for the material with a lower $(\Delta W/\Delta V)_c$ value. Stable crack growth has been assumed in this analysis, and in

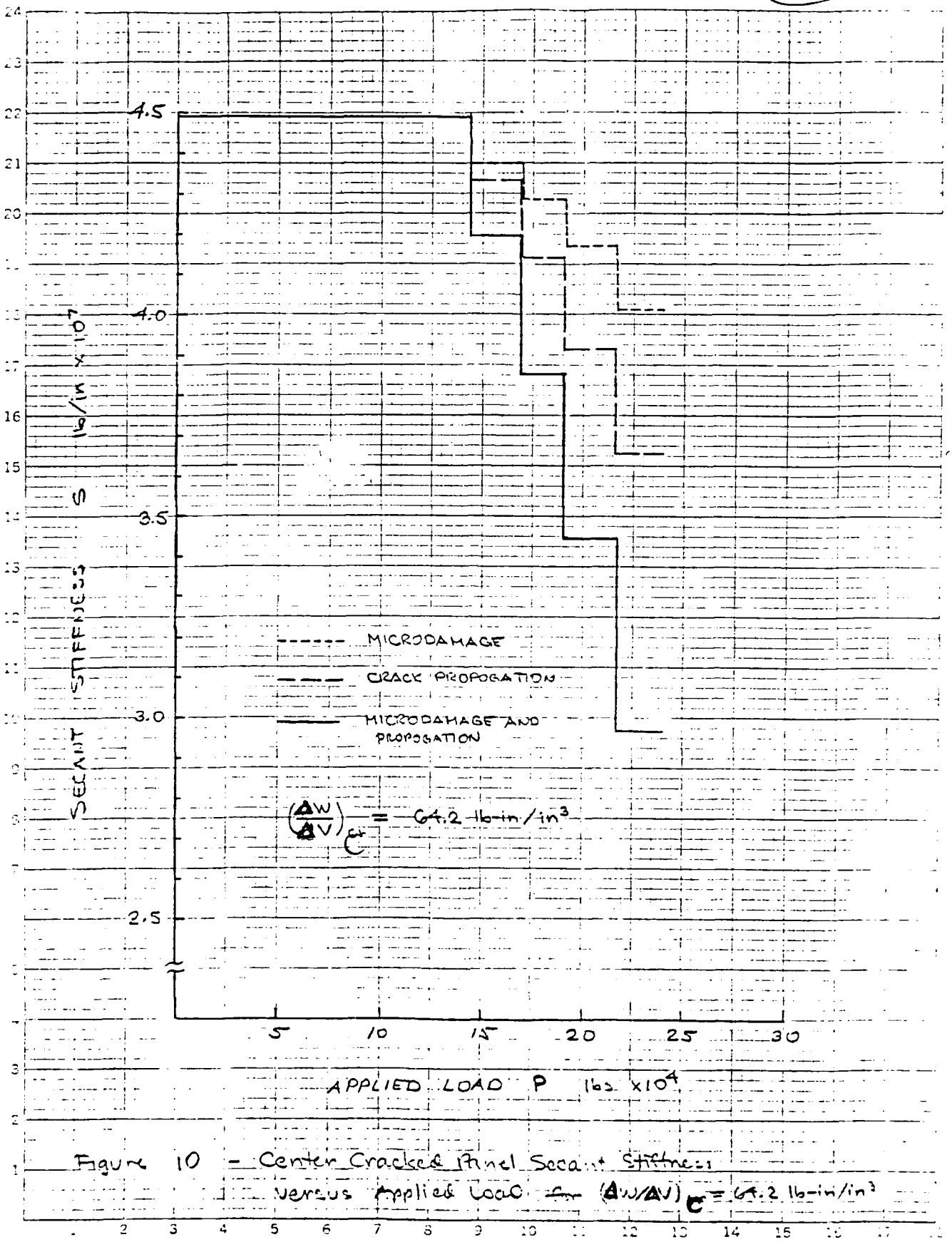

Figure 10 - Center Cracked Panel Secant Stiffness versus Applied Load for $(\Delta W/\Delta V)_c$ = 64.2 lb-in/in³

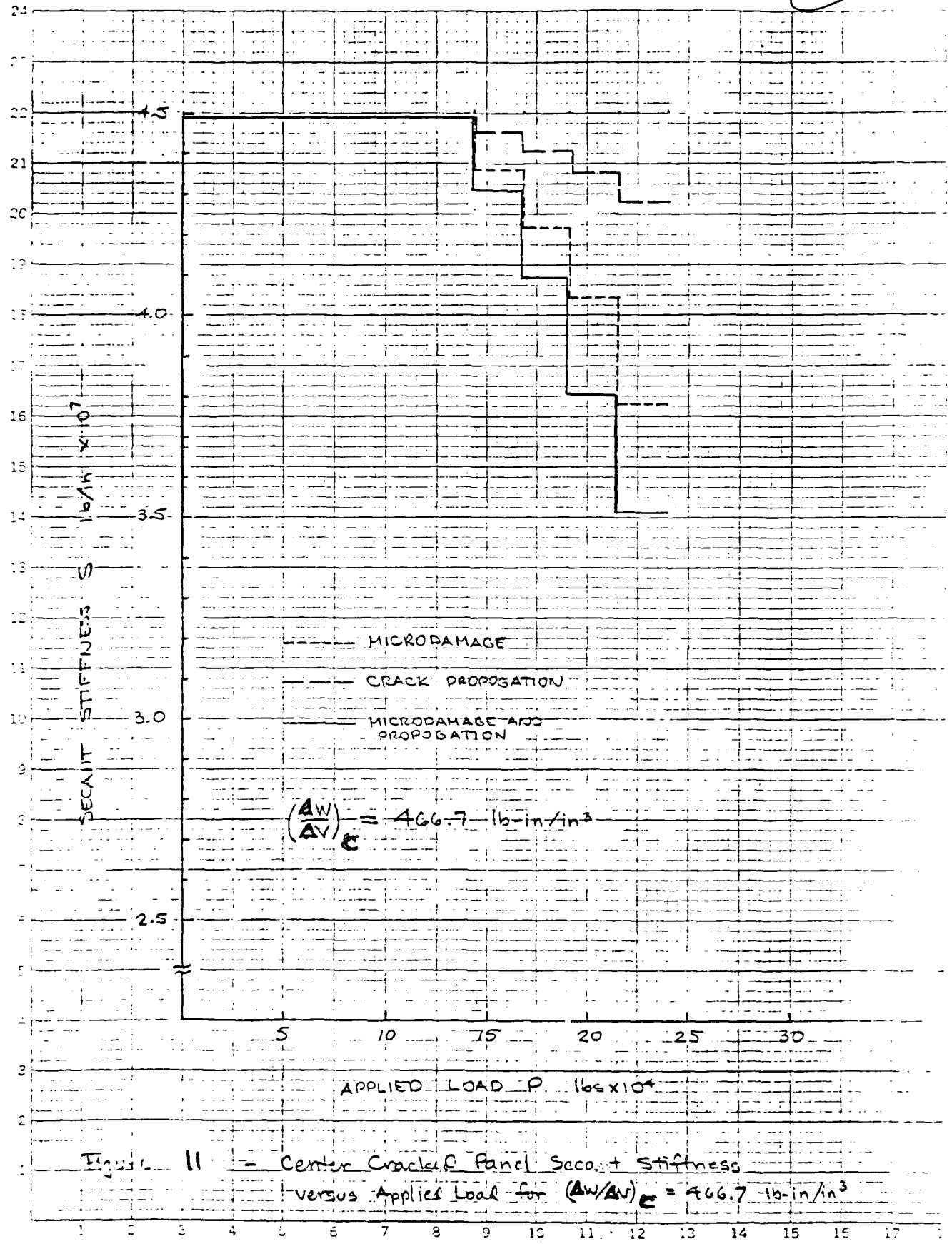

Figure 11 – Center Cracked Panel Secant Stiffness versus Applied Load for $(\Delta W/\Delta V)_{cr}$ = 466.7 lb-in/in³

(45)

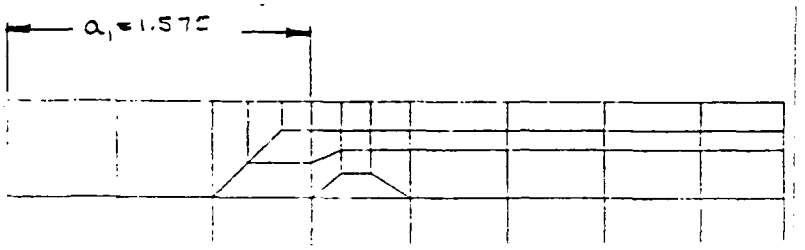

$P = 14.4 \times 10^4$ lbs

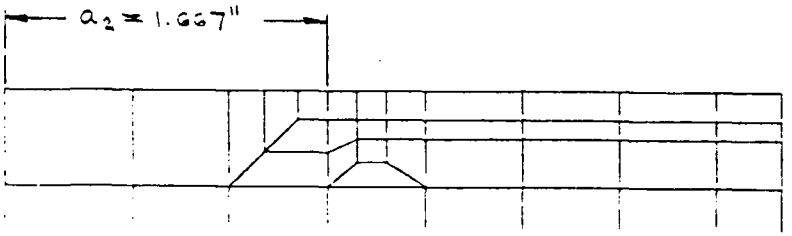

$P = 16.8 \times 10^4$ lbs

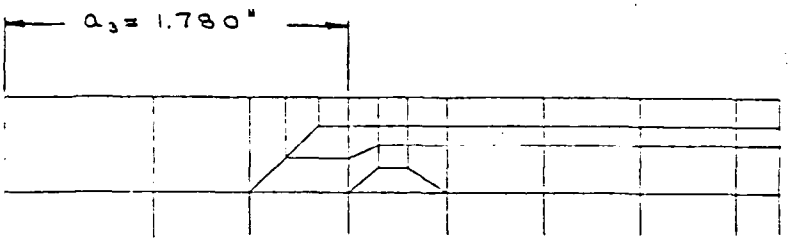

$P = 19.2 \times 10^4$ lbs

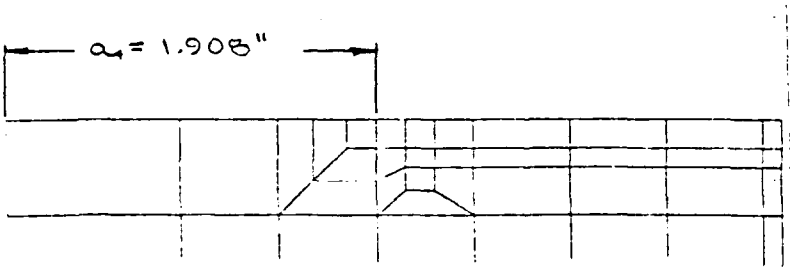

$P = 21.6 \times 10^4$ lbs

Figure 12 Crack Growth in the Absence of Microdamage for $(\Delta W/\Delta V)_c = 64.2$ lb-in/in^3

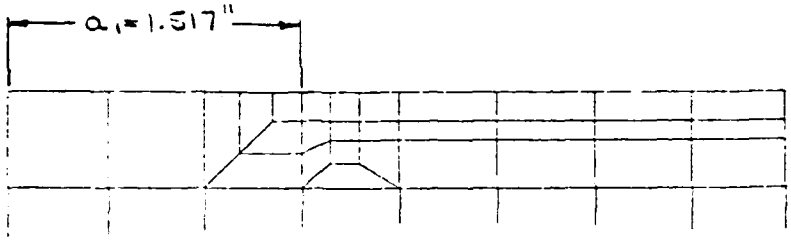

$P = 14.4 \times 10^4$ lbs

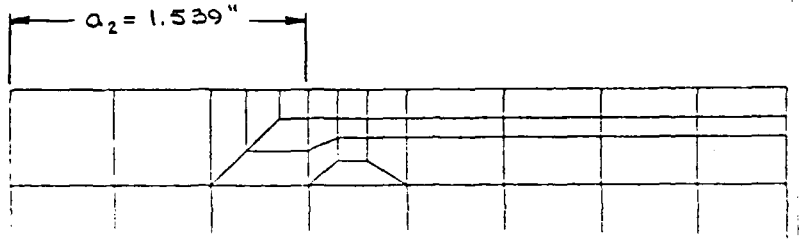

$P = 16.8 \times 10^4$ lbs

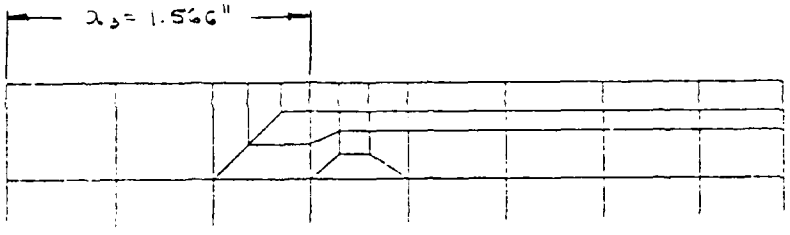

$P = 19.2 \times 10^4$ lbs

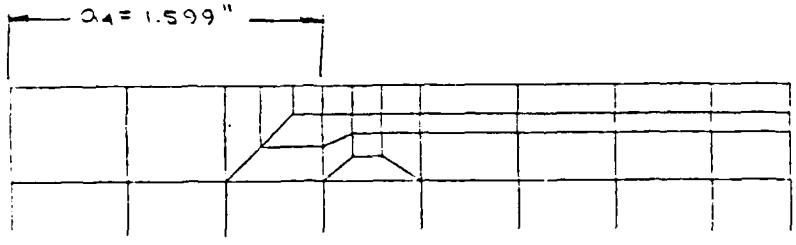

$P = 21.6 \times 10^4$ lbs

Figure 13 Macrocrack Growth in the Absence of Microdamage for $(\Delta U - \Delta V)_c = 46.7$ lb-in/in^3

all subsequent discussions involving crack growth.

The microdamage zones in the cracked specimens, as characterized by the original material elastic modulus of 30.0×10^6 psi and twenty-four damaged material states for the finite element discretization, are shown in Figures 14 and 15. Recall that material no. 25 is the highest level of damage in the discretization, with a tensile specimen secant modulus of 18.0×10^6 psi for a $(\Delta W/\Delta V)_c$ value of 64.2 lb-in/in^3, and 6.0×10^6 psi for a $(\Delta W/\Delta V)_c$ of 466.7 lb-in/in^3. All elements without a number are assumed to have not reached the yield condition, based on the average strain energy density taken over the element, and hence are material no. 1.

In Figures 16 and 17, the extent of microdamage is shown when crack propagation is also taken into consideration. No major differences in the damage zones for each material can be seen between a propagating and non-propagating macrocrack. There is some enhancement in the damage levels of the combined damage and crack propagation cases, as would be expected due to increasing macrocrack length. The damage zones in both cases, for both materials, are seen to be similar in the shape of "plastic enclaves" predicted by the von Mises criterion (which, as discussed above, is not based on microdamage, but rather traditional continuum mechanics), and observed in fracture specimens.

The crack growth increments shown above were determined according to the strain energy theory as discussed previously. The strain energy density fields ahead of the crack tip, with and without the effects of microdamage, at each load increment are shown in Figures 18 and 19. The predominant characteristics of these families of curves are the increasing intensity of the energy field for increasing crack lengths and the decreasing value of the relative critical strain

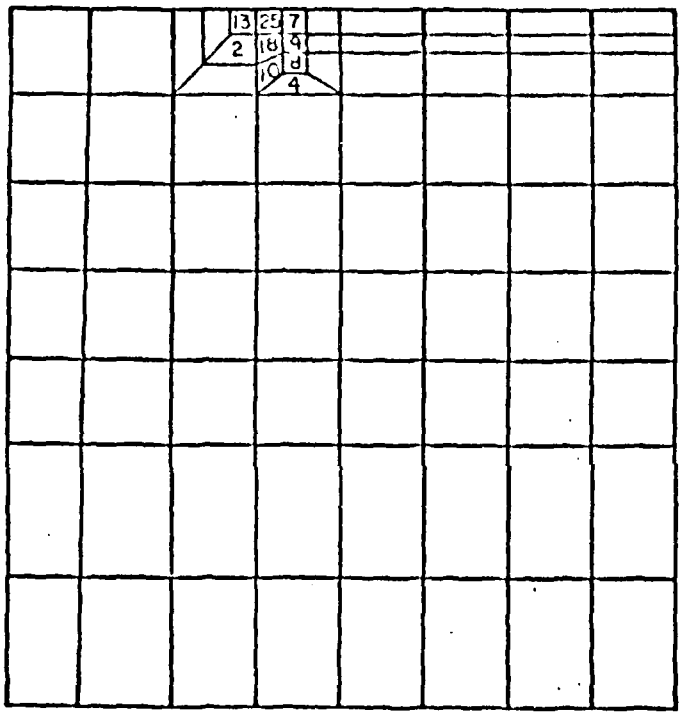

P = 14.4 x 10^4 lbs

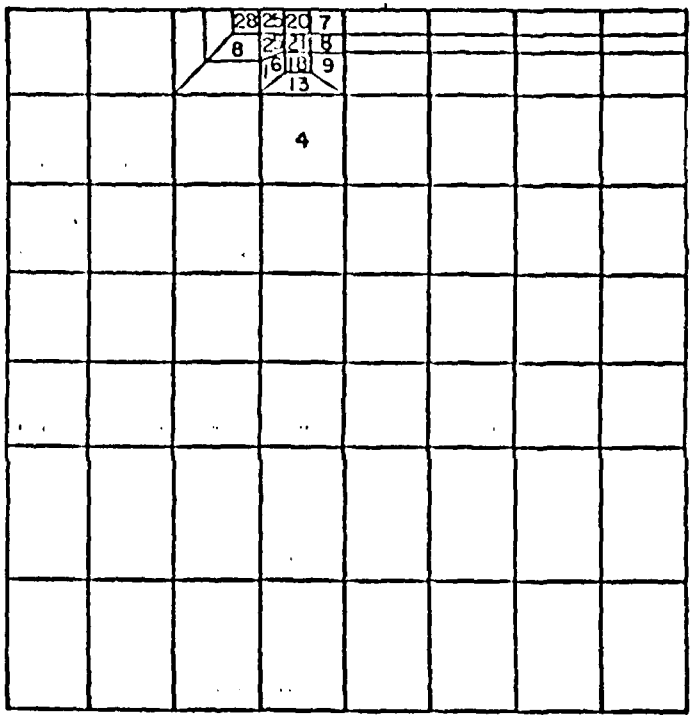

P = 16.8 x 10^4 lbs

blank ≡ MAT No. 1 (UNDAMAGED)

Figure 14 Hierarchy tree in the Absence of Macrocrack Growth for $(\Delta W/\Delta V)_c$ = 64.2 lb-in/in^3

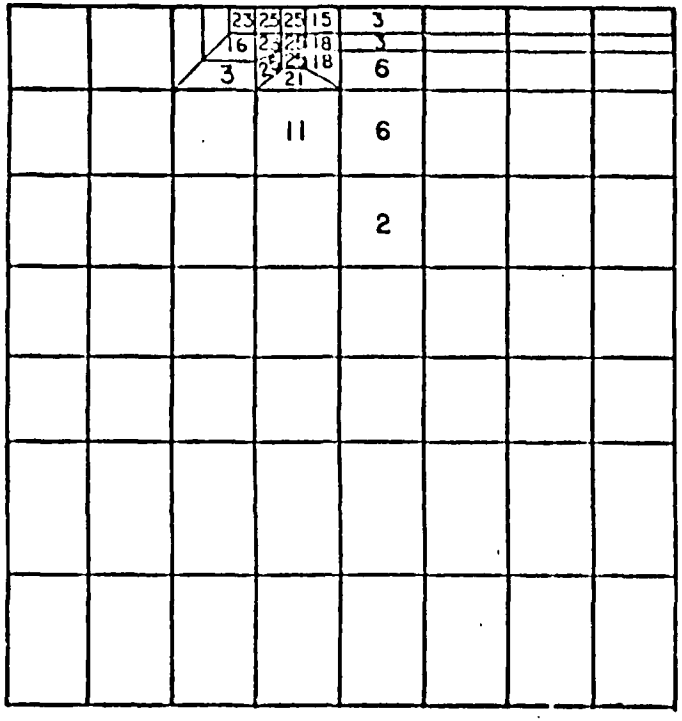

P = 19.2 x 10^4 lbs

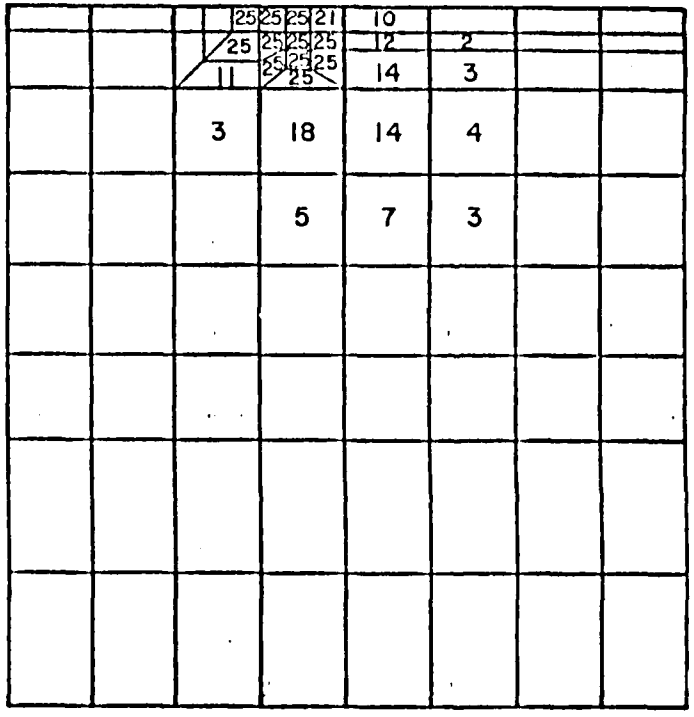

P = 21.6 x 10^4 lbs

blank ≡ MAT No. 1 (UNDAMAGED)

Figure 14 (continued) Microdamage Zones in the Absence of Macrocrack Growth for $(\Delta W/\Delta V)_{cr}$ = 64.2 lb-in/in^3

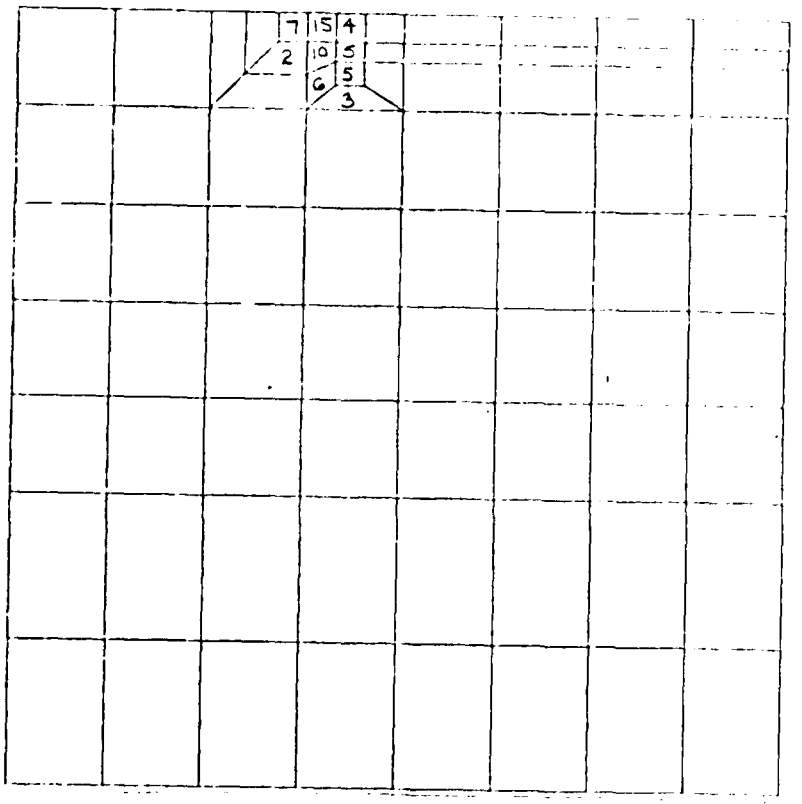

P = 14.4 x10⁴ lbs

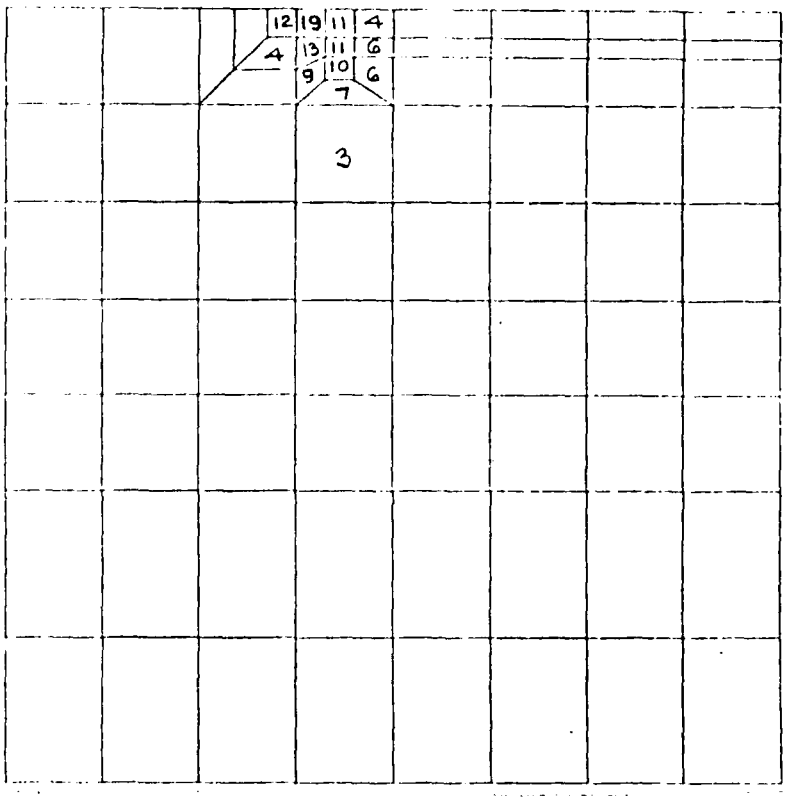

P = 16.8 x10⁴ lbs

blank ≡ MAT No. 1 (Undamaged)

Figure 15 Microdamage Zones in the Absence of Hoop [illegible]
Growth for $(\Delta W/\Delta V)_{cr}$ = -166.7 lb-in/in³

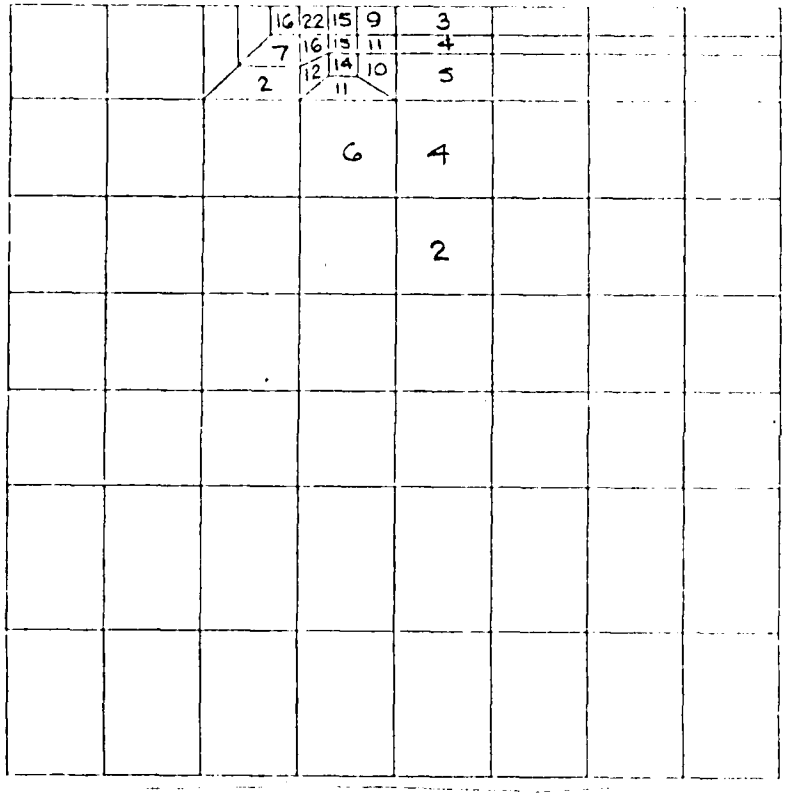

P = 19.2 x 10⁴ lbs

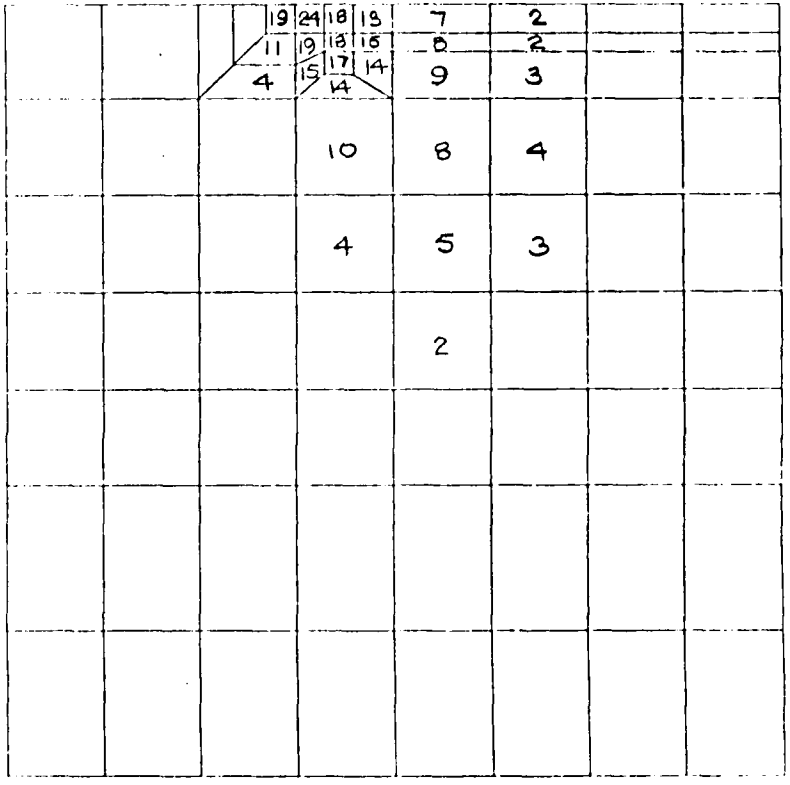

P = 21.6 x 10⁴ lbs

blank ≡ MAT No. 1 (Undamaged)

Figure 15 (continued) Maximum Shear Stress Zones in the Absence of Hemispherical [illegible]

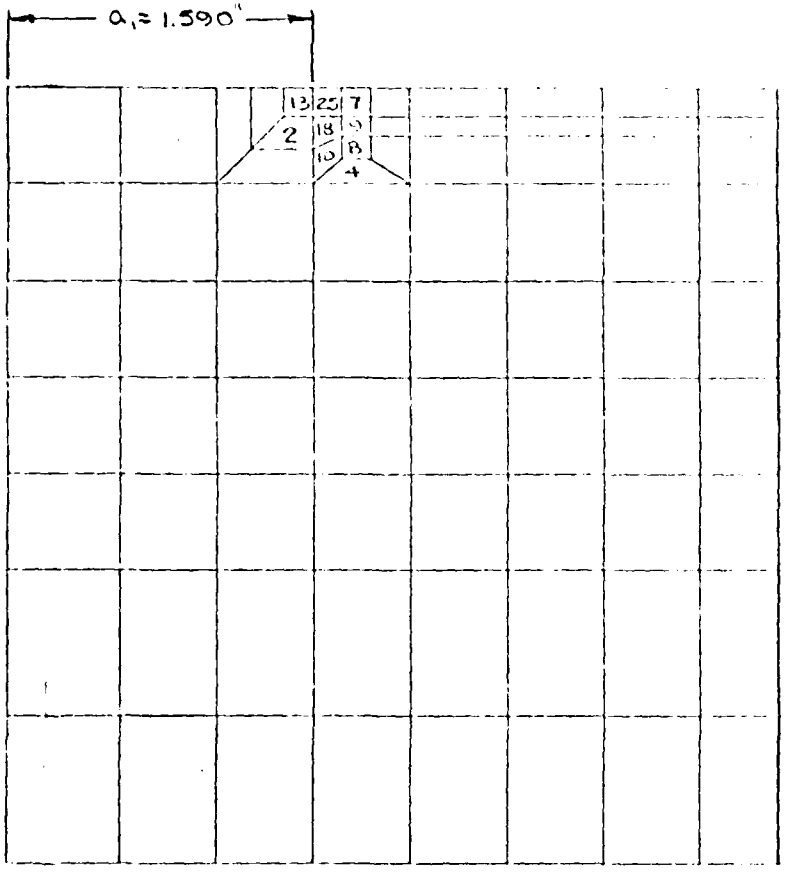

$P = 14.4 \times 10^4$ lbs

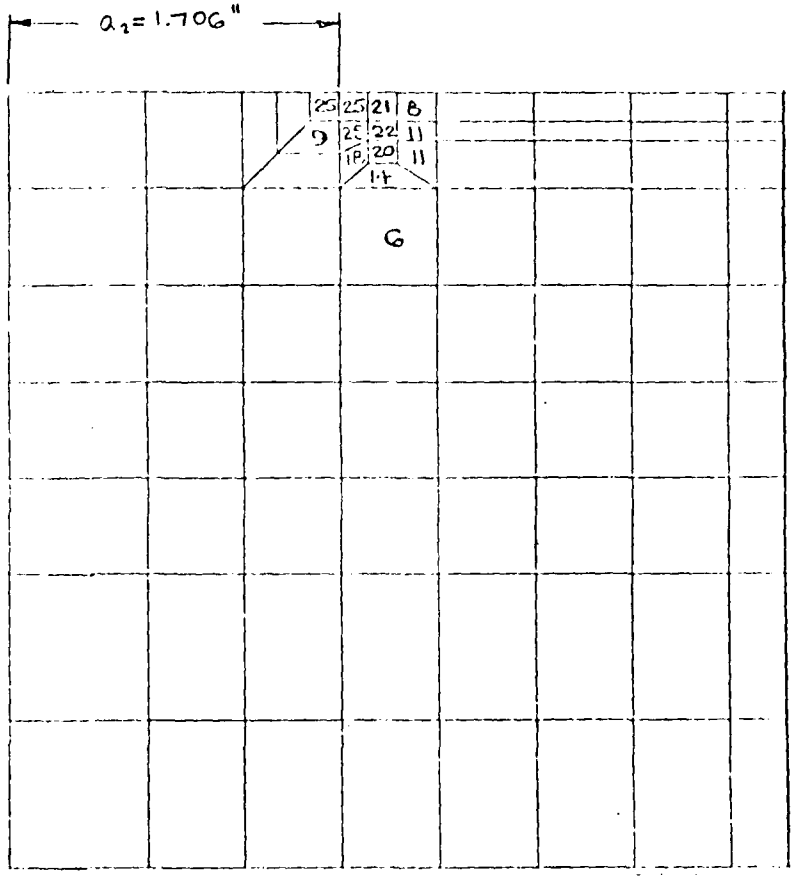

$P = 16.8 \times 10^4$ lbs

blank = Mat. No. 1 (Unbamaged)

Figure 16 Microdamage Zones a_1 & a_2 - Growth for $(\Delta W/\Delta V)_{cr} = 64.2$ lb-in/in^3

Marmarino

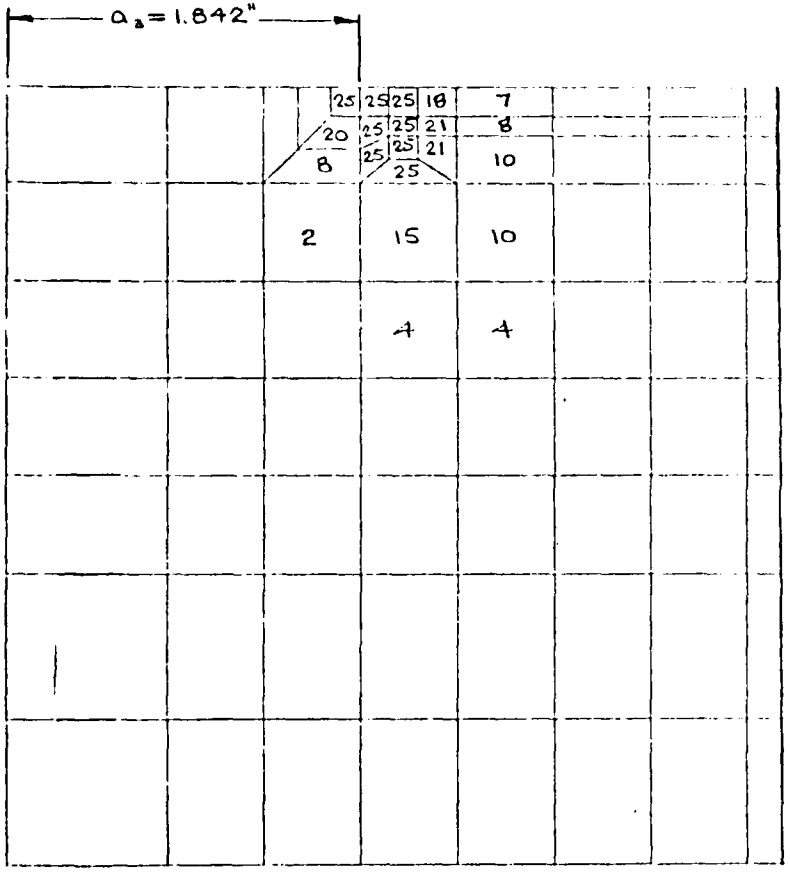

$P = 19.2 \times 10^4$ lbs

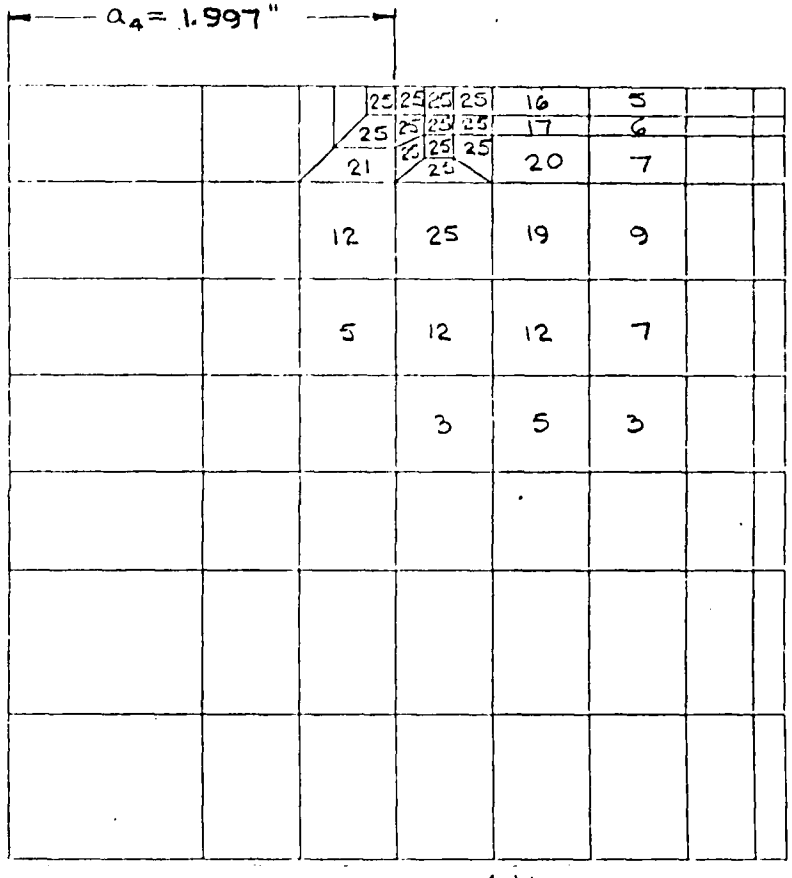

$P = 21.6 \times 10^4$ lbs

blank = Mat. No. 1 (Undamaged)

Figure 16 (continued) Microdamage Zone and Smooth for $(\Delta W/\Delta V)_{cr} = 64.2$ lb-in/in^3

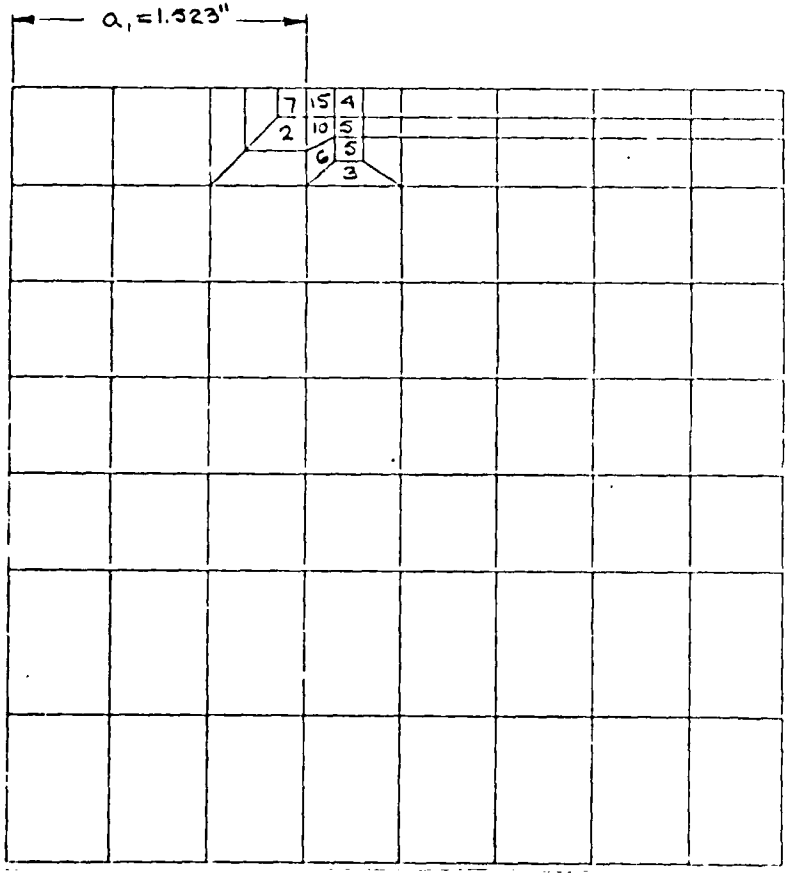

P = 14.4 x 10^4 lbs

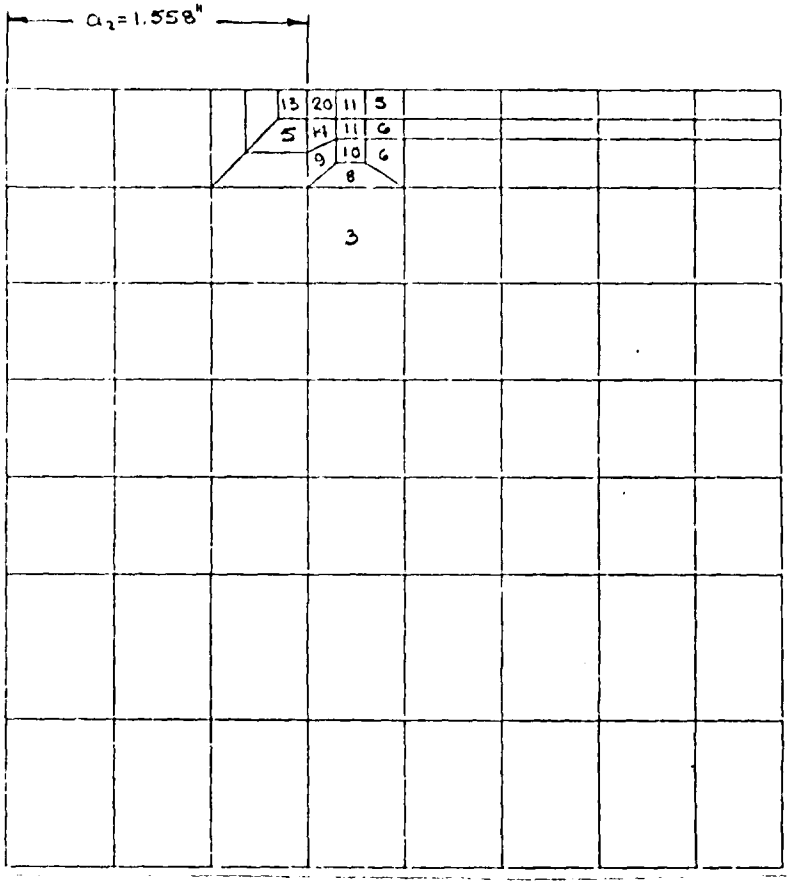

P = 16.8 x 10^4 lbs

blank = Mat. No. 1 (Undamaged)

Figure 17 Illustrating Zones and ... Growth for $(\Delta l/\Delta l)_{cr}$ = 466.7 lb-in/in^3

Macrocrack

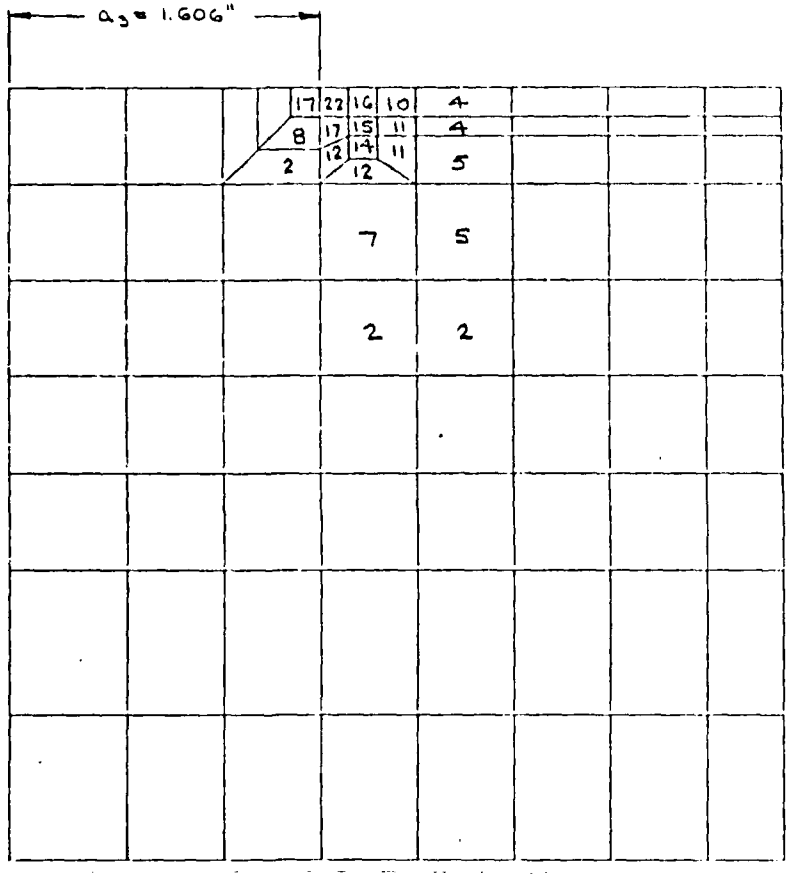

P = 10.2 x 10^4 lbs

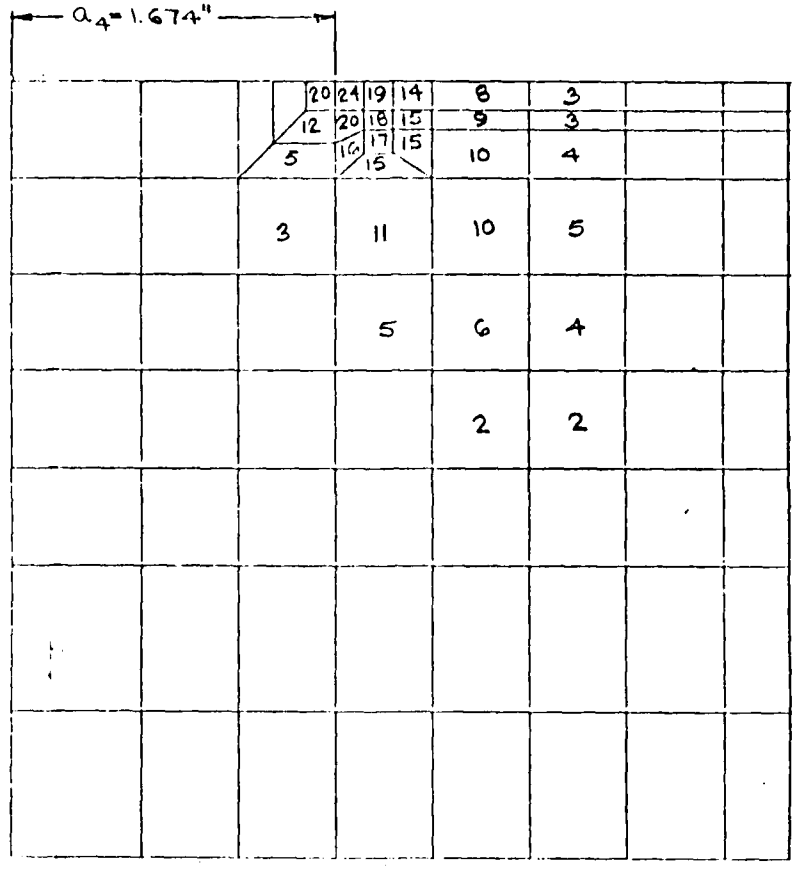

P = 21.6 x 10^4 lbs

blank ≡ Mat. No. 1 (Undamaged)

Figure 17(...) Microdamage zone and ... Growth for $(\Delta v_i/\Delta V)_c$ = 466.7 lb-in/in³

Macrocrack

(25) 8

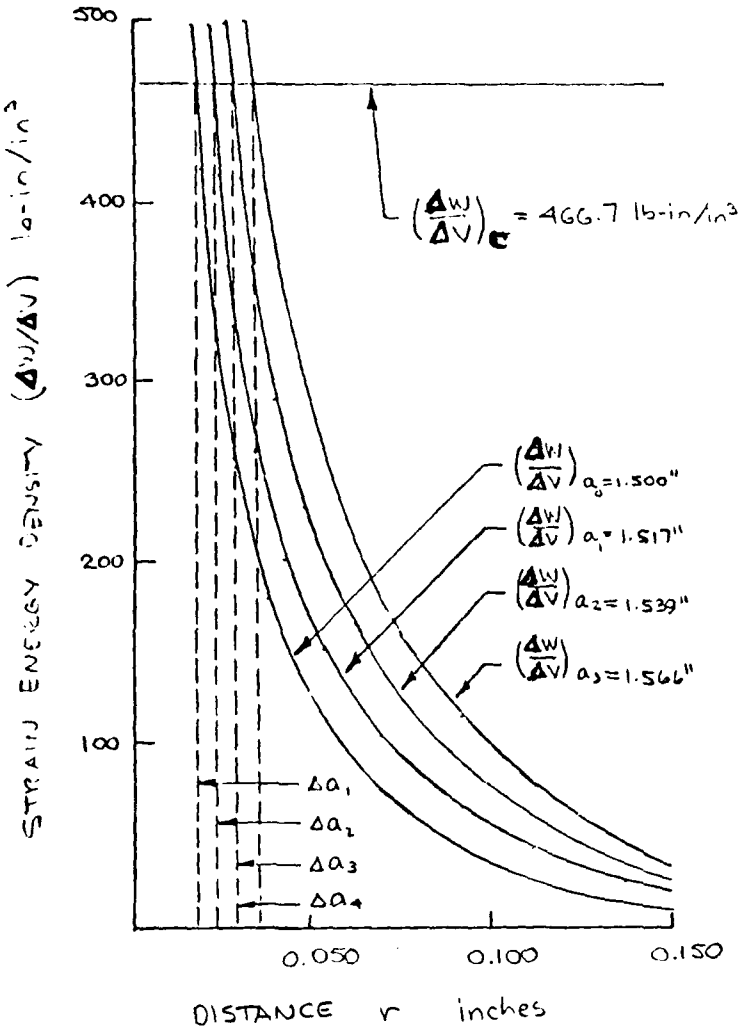

Crack increments without microdamage

$\Delta a_1 = 0.017"$
$\Delta a_2 = 0.022$
$\Delta a_3 = 0.027$
$\Delta a_4 = 0.033$

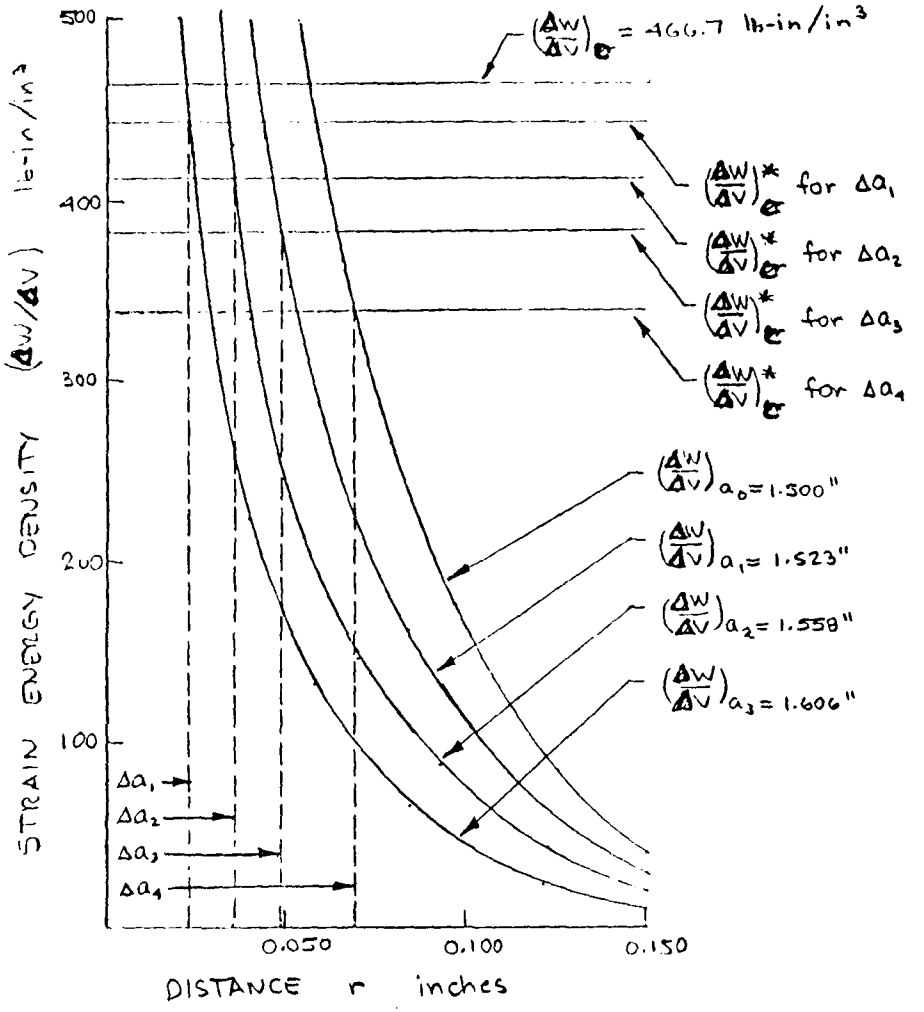

Crack increments with microdamage

$\Delta a_1 = 0.023"$
$\Delta a_2 = 0.035$
$\Delta a_3 = 0.048$
$\Delta a_4 = 0.068$

Figure 18 Strain Energy Density Ahead of Crack Tip for $(\Delta W/\Delta V)_c$ = 466.7 lb-in/in³

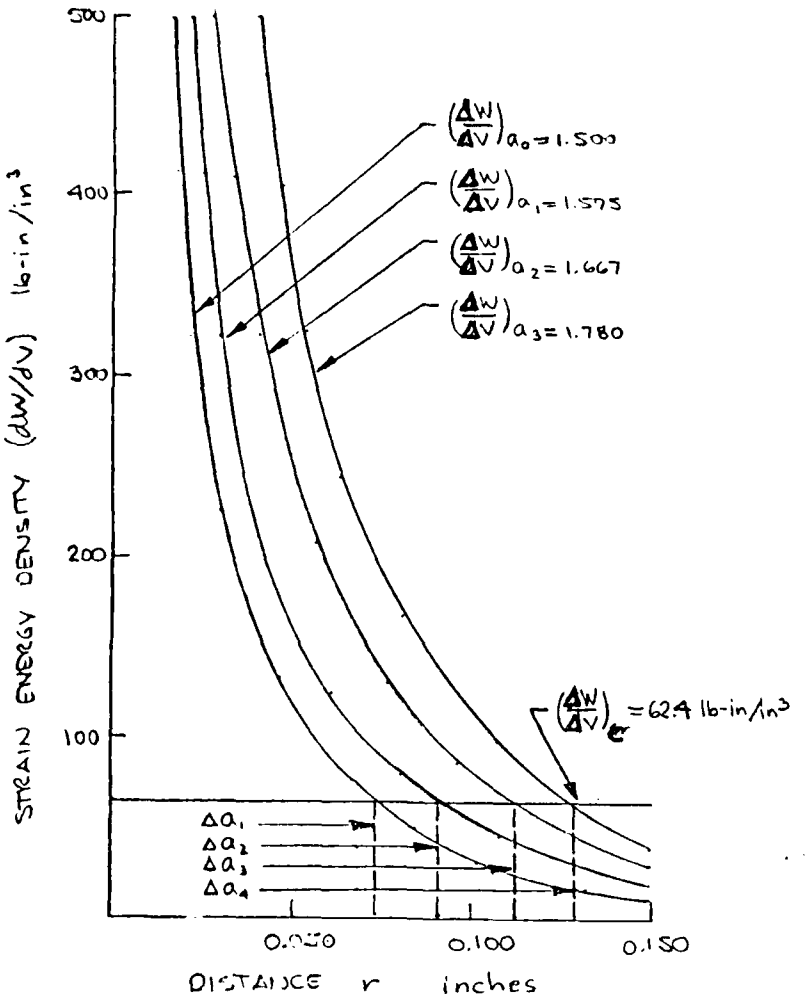

Crack increments without microdamage

$\Delta a_1 = 0.075"$
$\Delta a_2 = 0.092$
$\Delta a_3 = 0.113$
$\Delta a_4 = 0.128$

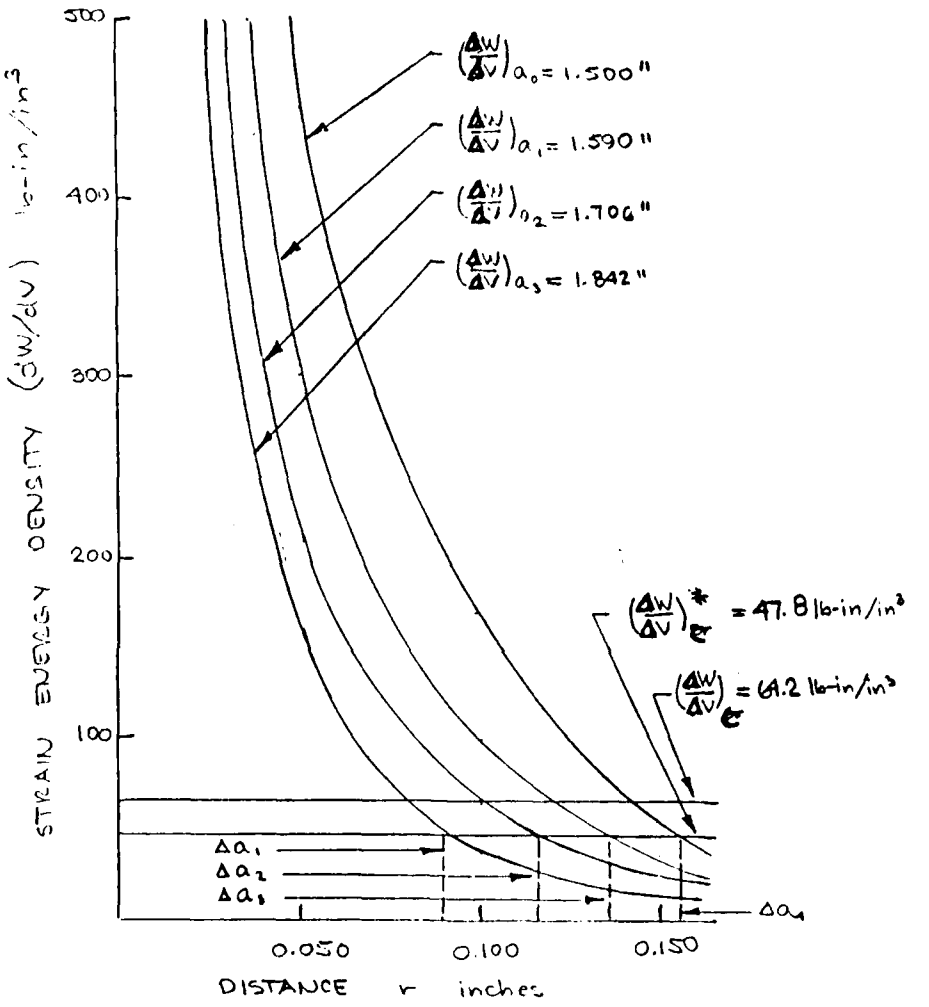

Crack increments with microdamage

$\Delta a_1 = 0.090"$
$\Delta a_2 = 0.116$
$\Delta a_3 = 0.136$
$\Delta a_4 = 0.155$

Figure 19 Strain Energy Density Ahead of Crack Tip for $(\Delta W/\Delta V)_{cr}$ = 64.2 lb-in/in³

energy $(\Delta W/\Delta V)_c^*$ as the damage level ahead of the crack tip increases. Due to the discretization of the panel domain required by the finite element method, the $(\Delta W/\Delta V)_c^*$ value is treated as a locally constant quantity in each individual element. This is, of course, similar to the way the elastic moduli of the individual elements are treated.

The average secant modulus in the microdamage zone is plotted as a function of load in Figure 20. For both materials, with and without macrocrack propaga-

Figure 20 - Average secant modulus in microdamage zone versus applied load

tion, the average secant modulus within the damage zone is seen to be between 83 and 88 percent of the undamaged value. This is interesting in light of the lowest values of the secant moduli characteristic of the two materials considered. These values are 0.6 and 0.2 times the undamaged modulus. The implication is that the effect of the higher levels of damage (particularly near the crack tip) on the average modulus are balanced by the lower levels of damage near the expanding periphery of the damage zone itself.

The damage center loci (Figure 21) for each material also show similar behavior. For loads less than 1.8×10^5 pounds, the loci follows the direction $\theta_o = \cos^{-1}(1-2\nu)$ of maximum strain energy density in the neighborhood of the crack tip, as discussed by Sih [4] for a linear elastic body. The departure of the loci from this direction occurs at applied loads greater than 1.8×10^5 pounds in the direction of the free surface. This is seen to be independent of the value of $(\Delta W/\Delta V)_c$, or whether macrocrack propagation is included as a dissipative mechanism. For the panel with a higher value of $(\Delta W/\Delta V)_c$, the movement of the loci away from the θ_o direction is seen to be greater than for the panel with the lower value of $(\Delta W/\Delta V)_c$. Thus, the increased dissipative capability characteristic of the higher $(\Delta W/\Delta V)_c$ material extends the damage zone toward the free surface. This relative movement of the damage zone may be related to the onset of stable and unstable macrocrack growth. It may be produced as the result of the damage zone size and geometry itself, the influence of the free surface ahead of the crack tip, or a combination of the above.

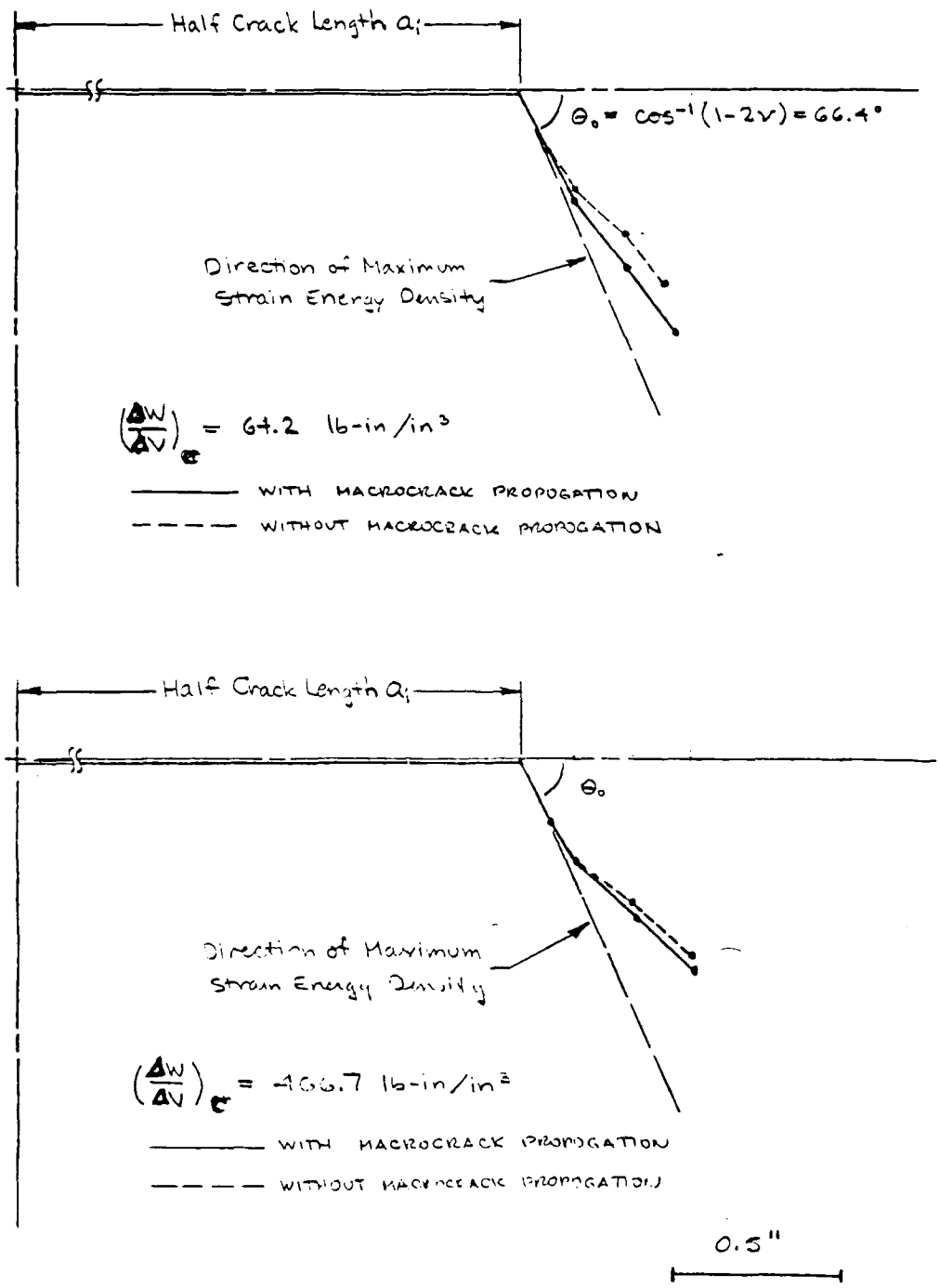

Figure 21 Damage Center Loci

CONCLUDING REMARKS

The global behavior of a center cracked specimen has been modeled by the finite element method while allowing for material damage at each load increment. Both microdamage (in the form of isotropic distributions of microcracks) and macrocrack propagation have been modeled by a consistent application of the strain energy density criterion. The thresholds of material damage are referred to data from the true stress-true strain curves of uniaxial tension tests.

The nonlinear behavior of the load-displacement curves for both separate and combined application of the microdamage and macrocrack propagation effects have been incrementally generated for two different materials as characterized by their critical strain energy density. Both the load-displacement curves and secant stiffness curves are material, specimen geometry and load configuration dependent. In this analysis, only the material properties of the cracked specimens have been changed in accordance with the severity of the damage. Conceptually, this approach could be applied to develop constitutive relations for materials in which damage due to micro and macrocracking can be treated. In particular, the procedure for a quantitative assessment of material damage in terms of load-displacement response has been established.

The results of the analyses show how macrocrack propagation can dominate the global nonlinearity when the critical strain energy density level is relatively low. Conversely, for the material with a higher critical strain energy density, the microdamage effect becomes more influential. These two observations are consistent with the generally observed results for materials that behave in a primarily brittle and primarily ductile fashion.

On the basis of the information obtained from the present analysis, coupled with additional and more refined damage models, appropriate tensile tests may be designed to reflect the damage processes which are actually occurring in the structural component. The appropriate choice of variables, which will be capable of describing the state of material damage, can then be incorporated into viable constitutive relations. These relations are useful for predicting the global behavior of structural members from material damage at the continuum scale.

BIBLIOGRAPHY

[1] Hertzberg, R. W., "Deformation and Fracture Mechanics of Engineering Materials", John Wiley and Sons, New York, New York, 1976.

[2] Banerjee, S., "Influence of Specimen Size and Configuration on the Plastic Zone Size, Toughness, and Crack Growth", Eng. Fract. Mech., 15, pp. 343-390, 1981.

[3] Shih, C. F. and German, M. D., "Requirements for a One-Parameter Characterization of Crack Tip Fields by the HRR Singularity", Int. Journal of Fract., 17, pp. 27-43, 1981.

[4] Sih, G. C., "A Special Theory of Crack Propagation", Methods of Analysis and Solution of Crack Problems, G. C. Sih, ed., Noordhoff, Leyden, pp. XXI-XLV, 1973.

[5] Sih, G. C. and Cha, B. C. K., "A Fracture Criterion for Three Dimensional Crack Problems", Eng. Fract. Mech., 6, pp. 699-723, 1974.

[6] Sih, G. C. and Matic, P., "Mechanical Response of Materials with Physical Defects, Part 1: Modeling of Material Damage for Center Cracked Panel", Institute of Fracture and Solid Mechanics Tech. Rept. AFOSR-TR-81-1, 1981.

[7] Hilton, P. D., Gifford, L. N. and Lomacky, O., "Finite Element Fracture Mechanics of Two Dimensional and Axisymmetric Elastic and Elastic-Plastic Cracked Structures", Naval Ship Research and Development Center Report No. 4493, 1975.

[8] Hutchinson, J. W., "Singular Behavior at the End of a Tensile Crack in a Hardening Material", J. Mech. and Physics of Solids, 16, pp. 13-31, 1968.

[9] Rice, J. R. and Rosengren, G. F., "Plane Strain Deformation Near a Crack Tip in a Power Law Hardening Material", J. Mech. and Physics of Solids, 16, pp. 1-12, 1968.